POLITECNICO
MILANO 1863

SCUOLA DI INGEGNERIA INDUSTRIALE
E DELL'INFORMAZIONE

Development of a Maneuver Optimization Tool for a Space Based Debris Observation Mission

Master of Science in
Space Engineering - Ingegneria Spaziale

Author: **Mattia Ricci**

Student ID: 977069
Advisor: Prof. Pierluigi Di Lizia
Co-advisor: Samira Hosseini
Academic Year: 2022-23

Abstract

The following work aimed at the development of a maneuver optimization tool for the Flamingo pilot satellite, considering operational constraints imposed. Minimization of the fuel consumed for the LTAN correction maneuver will mainly be investigated. The basis for the analysis is drawn from the Edelbaum optimum solution for low-thrust maneuvers, along with Kechichian's extension. The tool will be developed combining the MATLAB and GMAT software, driving the different optimization techniques exploited and the ability to implement spacecraft architectures. Eclipse events and perturbations will be accounted for in the analysis to provide a full robust model of the low-thrust maneuver. Two different propulsion systems will be considered, specifically electric and chemical, to provide a basis for the selection of the propulsion system and mass budget for the mission.

Keywords: Orbital Maneuvers, Maneuver Optimization, Low-Thrust Propulsion Systems, Extended Edelbaum Method, Optimal Control Problem

Abstract in lingua italiana

Lo studio condotto riguarda la creazione di uno strumento per ottimizzazione di manovre da condurre per un satellite, considerando dei vincoli dati da operazioni da svolgere durante la missione. La discussione verte sulla minimizzazione del consumo di propellente per la correzione della LTAN. Le basi per lo studio della manovra sono investigate dal lavoro fatto da Edelbaum, trovando le condizioni per la soluzione ottimale, a cui si aggiunge l'estensione con l'optimal control problem, operata da Kechichian. Una cooperazione tra i software MATLAB e GMAT viene sfruttata, servendosi delle diverse tecniche di ottimizzazione dei due. Condizioni di eclisse e perturbazioni varie sono prese in considerazione per creare uno strumento che sia il più robusto possibile. Differenti sistemi propulsivi saranno poi investigati, cercando di trovare una base per l'uso di uno dei due per la missione.

Keywords: Manovre Orbitali, Ottimizzazione di Manovre, Sistemi di Propulsione a Bassa Spinta, Metodo di Edelbaum Esteso, Controllo Ottimale

Contents

List of Figures

List of Tables

Nomenclature

Acronyms and Abbreviations

CAM	Collision Avoidance Manoeuvre
DC	Duty Cycle
EEM	Extended Edelbaum Method
GEO	Geosynchronous Earth Orbit
GG	Gravity Gradient
GUI	Guide User Interface
IADC	Inter-Agency Space Debris Coordination Committee
LEO	Low Earth Orbit
MEO	Medium Earth Orbit
NLP	Non Linear Programming
OCP	Optimal Control Problem
SES	Split Edelbaum Sequence
SK	Station Keeping
SP	Short Periodic
SQP	Sequential Quadratic Programming
SRP	Solar Radiation Pressure
SSO	Sun-Synchronous Orbit
SST	Space Surveillance Tracking

Physical quantities

α	In-plane angle	$[^\circ]$
β	Out-of-plane angle	$[^\circ]$
$\boldsymbol{a}_d$	Drag Acceleration	$[m/s^2]$
γ	Shadow Percent	$[-]$
λ	Latitude	$[^\circ]$

μ	Gravitational parameter	$[km^3/s^2]$
ν	Eclipse Factor	$[-]$
Ω	RAAN	$[^\circ]$
ω	Argument of Periapsis	$[^\circ]$
ϕ	Longitude	$[^\circ]$
ρ	Density	$[Kg/m^3]$
θ	True Anomaly	$[^\circ]$
θ_C	Eclipse Center	$[rad]$
θ_{SH}	Earth Shadow Angle	$[rad]$
A	Area	$[m^2]$
a	Semi-major axis	$[km]$
AoL	Argument of Latitude	$[^\circ]$
C_d	Drag Coefficient	$[-]$
C_r	Reflectivity Coefficient	$[-]$
e	Eccentricity	$[-]$
f	Thrust acceleration	$[kg]$
i	Inclination	$[^\circ]$
I_{sp}	Specific Impulse	$[s]$
$LTAN$	Local Time of the Ascending Node	$[h]$
M	Mean Anomaly	$[^\circ]$
m	mass	$[kg]$
r	Distance	$[km]$
R_e	Earth radius	$[km]$
T	Thrust	$[N]$
t	time	$[s]$
U	Gravitational Potential	$[s]$

v	Velocity	$[km/s]$

1 Introduction

1.1. Background and Motivation

Space-based debris observation missions have become increasingly more important in recent times due to their growing amount in Earth's orbits. The enormous and continuous threat caused by these object can lead to critical spacecraft damage that can compromise the mission or even to its complete failure. It is, therefore, imperative to pose a limit to the menaces created by space debris.
The creation of augmented debris catalogues in the most crowded regions is the first step to make to provide an effective solution to the problematic, and that's how debris observation missions will help to solve the problem.
In-space telescopes mounted on satellites will provide tracking of most of the objects present in the crowded regions, leading to a significant improvement of the debris catalogues. Of course to make this possible, on-board mounted technologies must operate within a specific framework to reach the best performances achievable.
In order to do this, the spacecraft must be inserted in its nominal operational orbit, defined by the nominal altitude, inclination and orientation which should provide the best performances with respect to the mounted payload and the tracked object category (mainly performances depend on the size of the objects tracked). In this regard, an efficient and effective method for maneuver planning must be developed, aiming for minimum fuel consumption and minimum transfer time.
In particular, transfer time reduction leads to a drastic reduction of the costs, since a longer duration of the maneuver implies the involvement of a number of other operations that have to be executed for a longer time, also in terms of fuel allocation.
The design of such methods can significantly improve the accuracy and the effectiveness of the mission, allowing also a broader application in other areas of space exploration, including satellite servicing and formation flying.
Lastly, the increase in flexibility gained with the optimization allows to define alternative maneuver strategies in situations where the mission requirements change, or where unexpected events occur.
Of course, a lot of compromises have to be met, forcing us to privilege some aspects and neglecting other ones. The trade-off between the perfect situations and the cost necessary

is always the major question to which the best answer has to be provided.

1.2. About Vyoma and Space Situational Awareness

1.2.1. Space is a risky place

More satellites are being launched today than ever before, driven also by the incredible rise of private companies in the latest period. This means that the commercial orbits in which most of the satellite operate are becoming really overcrowded, either by currently functioning satellites or by old ones, no more in activity.
The annual Space Environment Report published by ESA [1] puts really a figure on the current situation of the Debris orbiting around the Earth. Based on the models developed by ESA, it is estimated that the number of total objects larger than 1 cm in size is likely to be over 1 million.
The figures here reported (Figure A.2a, A.2b) are extracted by this document, providing an overview of the current space environment. The problem posed by space debris is then a significant risk for the safety and sustainability of space activities. In the long term, in fact, this could lead to the so called "Kessler Syndrome" [2], a scenario in which the collision of two objects in orbit generate a large number of smaller fragments, which, in turn, collide with other objects, creating more debris, continuing exponentially, leading to a cascade effect.
This is particularly true in the case of common operational orbits in which most of the spacecraft are placed, as in the GEO or LEO. The latter, in particular, has seen a huge growth in the last period due to the launch of several constellations used by private companies for internet connection, along with more common Earth observation satellites.
Thankfully, current companies have become more sensible about this issue, and a large number of them is investing in space-debris mitigation, trying to overcome this problematic.
This is possible also thanks to the restrictive guideline introduced by the IADC [3], which establishes how the mission should be conceived from the early concept to the disposal phase, in which the spacecraft is no more operational. As a matter of fact, over 40 years of unruled space activities led to the current situation where we face congested orbits and a harmful of other problematics. The design and mission profile of a spacecraft, estimation and limitation of accidental collision with catalogue objects are then mandatory. In-space maneuvering is also affected by this, as periodic Collision Avoidance Manoeuvre have to be conceived in order to prevent catastrophic events.
Ultimately, accidental break-ups or subsystem malfunctioning have to be also considered,

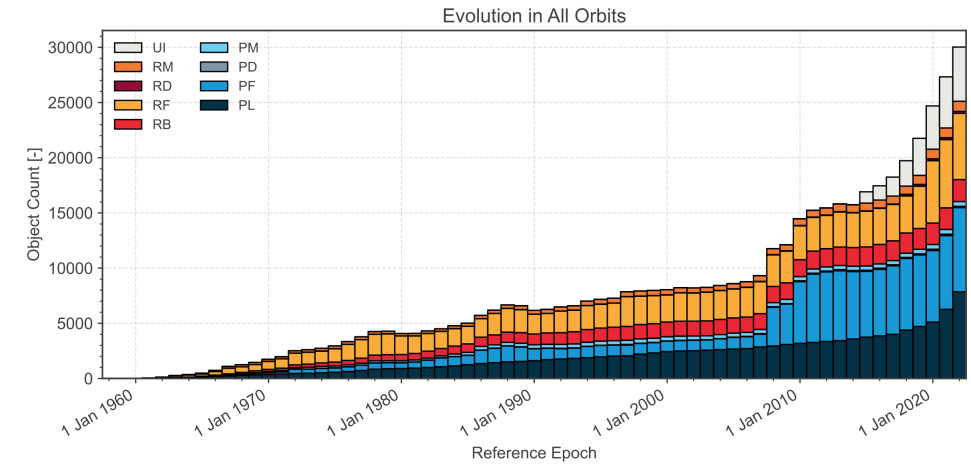

(a) Total number of object by class

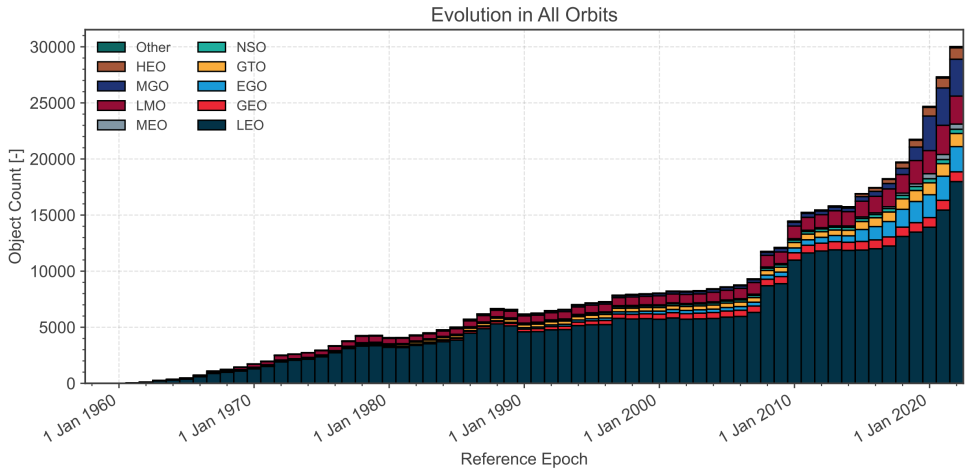

(b) Total number of object by orbit

Figure 1.1: Evolution of the total number of objects divided by class and by orbit

as adequate measures have to be taken, otherwise disposal measures should be conducted.

1.2.2. Space Debris

The term "Space Debris" [4] indicates, by definition, any artificial material orbiting the Earth that is no longer functional. They are mainly generated during normal operations as a satellite is being inserted in orbit, for example by the injection of stages, the release of mission-related objects and the eventual retirement of a satellite itself. Additional sources of debris can be subsequent break-ups and other events that lead to the release of material.

Of course, not only small size objects are present, but also larger objects have been catalogued, such as spacecraft that ended their operational time as well as rocket stages. To

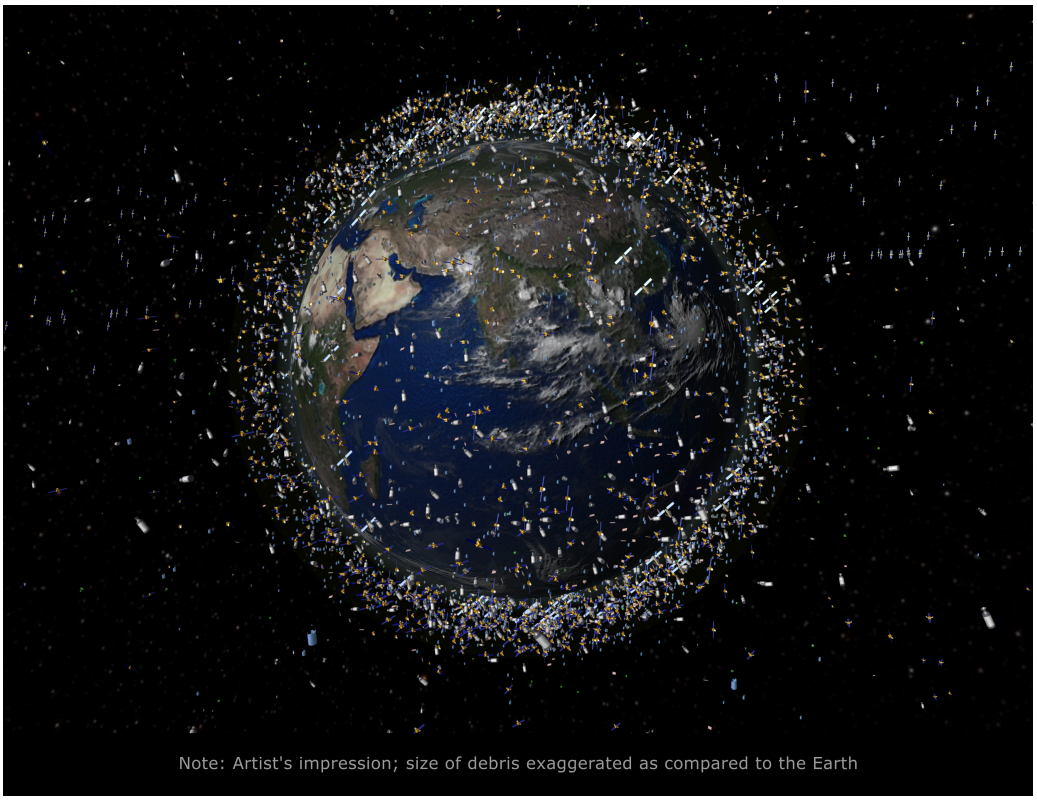

Figure 1.2: Low-Earth Orbit Debris Objects

provide the total number of objects orbiting in space, existing catalogue are not sufficient. Statistical models have then been used to provide an estimation of the quantity of debris present in space. The last update on the total amount of space objects orbiting the Earth [5] divided by class is provided in Table 1.1.

Dimension	**Number of objects**
$>$ 10 cm	36500
1-10 cm	1000000
$\leq$ 1 cm	130 mln

Table 1.1: Number of objects in space with respect to their dimensions

Space-related debris can be divided [1] in two categories: the ones which can be traced back to a specific launch event with a well-defined nature and the ones untraceable. The last ones are defined as "Unidentified", whereas the first ones as:

- Payloads, space object designed to perform a specific function in space excluding

[1] Class division of space-debris is purely reported from the [1]

launch functionality. This includes operational satellites as well as calibration objects.

- Payload mission related objects, space objects released as space debris which served a purpose for the functioning of a payload. Common examples include covers for optical instruments or astronaut tools.
- Payload fragmentation debris, space objects fragmented or unintentionally released from a payload as space debris for which their genesis can be traced back to a unique event. This class includes objects created when a payload explodes or when it collides with another object.
- Payload debris, space objects fragmented or unintentionally released from a payload as space debris for which the genesis is unclear but orbital or physical properties enable a correlation with a source.
- Rocket body, space object designed to perform launch related functionality; This includes the various orbital stages of launch vehicles, but not payloads which release smaller payloads themselves.
- Rocket mission related objects, space objects intentionally released as space debris which served a purpose for the function of a rocket body. Common examples include shrouds and engines.
- Rocket fragmentation debris, space objects fragmented or unintentionally released from a rocket body as space debris for which their genesis can be traced back to a unique event. This class includes objects created when a launch vehicle explodes.
- Rocket debris, space objects fragmented or unintentionally released from a rocket body as space debris for which the genesis is unclear but orbital or physical properties enable a correlation with a source.

Of course, as space missions span across several orbit types, the distribution should be very different. However, the presence natural cleaning mechanisms, such as perturbations to the orbital motion due to the Sun and Moon, forces induced by air drag or several other type of similar disturbances, lead to maximum debris concentrations at certain altitudes such as 800–1000 km range and near to 1400 km. Furthermore, LEO satellites are continuously exposed to drag resistance and, depending on the altitude, after a few weeks, years or even centuries, it will decelerate the satellite sufficiently that it reenters Earth's atmosphere. This general rule is not valid at higher altitudes (above 700–800 km) where the air drag is less powerful and objects generally remain in orbit for at least several decades.

Secondary peaks of spatial densities in GEO (Geostationary Orbit), at 35 786 km altitude and near the orbits of navigation satellite constellations between 19 000 and 23 000 km altitude in MEO (Medium Earth Orbit) are smaller by two to three orders of magnitude.

1.2.3. Vyoma

Within this context, it is worth to mention the work that Vyoma is putting to limit the entity of the problem.
Vyoma is a space company that strives to ensure safety and sustainability of space operations by providing critical infrastructure. Combining satellite cameras and machine learning automation services it enables real-time mapping of space objects and safe satellite operations.
In this way, Collision avoidance maneuver and orbit determination can be provided, ensuring the safety of any satellite operation.
Vyoma therefore aims to establish itself as a reliable provider of space surveillance and tracking (SST) services and data for satellite operators and owners. The data collected by the satellite constellation, along with its advanced tools and software, has the potential to revolutionize the satellite industry.

1.3. Thesis Scope and Structure

The purpose of the work is to develop a general tool for the optimization of the maneuver for the Flamingo Pilot satellite orbiting in a 500 km Sun Synchronus Orbit. The focus will be on the LTAN change that has to be performed to put the satellite in the best conditions for the payload to operate.
Two different propulsion systems will be analyzed (chemical and electric) in order to establish the best subsystem that could fit for the purpose.
Chapter 2 will frame the orbit scenario in terms of perturbations and eclipses events. The review of the state of the art for the transfer in Chapter 3 includes the classic Edelbaum Transfer and the Extension of the transfer made by Kechichian and Kluever, along with the optimal control problem and an overview of the propulsion systems.
Chapter 4 will present the optimization process, illustrating how the maneuver is implemented, in both the GMAT and MATLAB software, showing how the two are linked together.
Finally, a presentation of the results achieved in terms of fuel optimal condition is carried out, with a discussion of the impact they have on the mission.

The work is then extended, considering the impact of the maneuver on the overall mission lifetime (lasting approximately 5 years): in this frame Station Keeping maneuver have to be implemented, both following guidelines for the orbit maintenance and not to compromise the payload performance. The work however is still in progress, so results will not be presented, but the outline of the maneuver required will be evaluated.

2 | Theoretical Framework

The investigated operational orbit is a 500 km sun synchronous orbit, whose parameters referring to the insertion coordinate [1] are reported in Table 2.1.

Starting Epoch	**a** [km]	**e** [-]	**i** [°]	**Ω** [°]	**ω** [°]	**θ** [°]
19 Oct 2023 23:59:00	6903	0	97.5	187.5	0	0

Table 2.1: Insertion Orbit Parameters

Orbit insertion will be provided by a carrier[2], which shall provides a determined range of uncertainty in which the insertion will be granted. As a matter of fact, uncertainty interval considered for the analysis is:

Orbit Parameter	**Uncertainty Range**
SMA (a)	± 25 km
Inc (i)	± 0.1 °
RAAN (Ω)	± 0.2 °

Table 2.2: Uncertainty Ranges for insertion orbit

After the deployment of the satellite from the carrier the actual LTAN correction maneuver can't take place immediately, as a certain time period for what it's called the "commissioning phase" [6] must be considered. In this scenario all the subsystems, including the payload, must be switched on, establishing a communication with the ground centre to check the functionality of the satellite, as the standard procedure requires.
The duration of this early part of the mission is still unknown (usually lasts for 1-2 months) as there may incur some problems or some subsystems malfunctioning requiring additional operations, but, as a preliminary design, the duration is set to 60 days [3].

[1] Assumptions have been made on some of the parameters (e, ω, θ)

[2] No information is provided as the launch date and the launch carrier are still unknown, so assumptions are made on a worst-case scenario or rather a maximum allowed range is required

[3] Additional requirements may arise from regulations, further considerations have to be taken into account

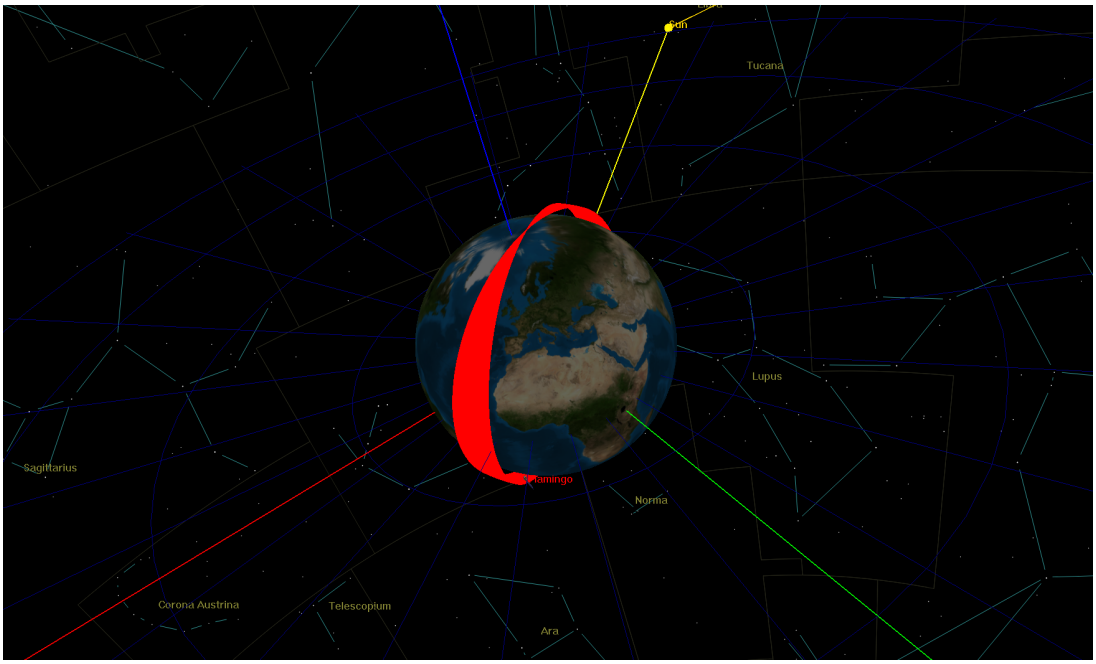

(a) Orbit Representation

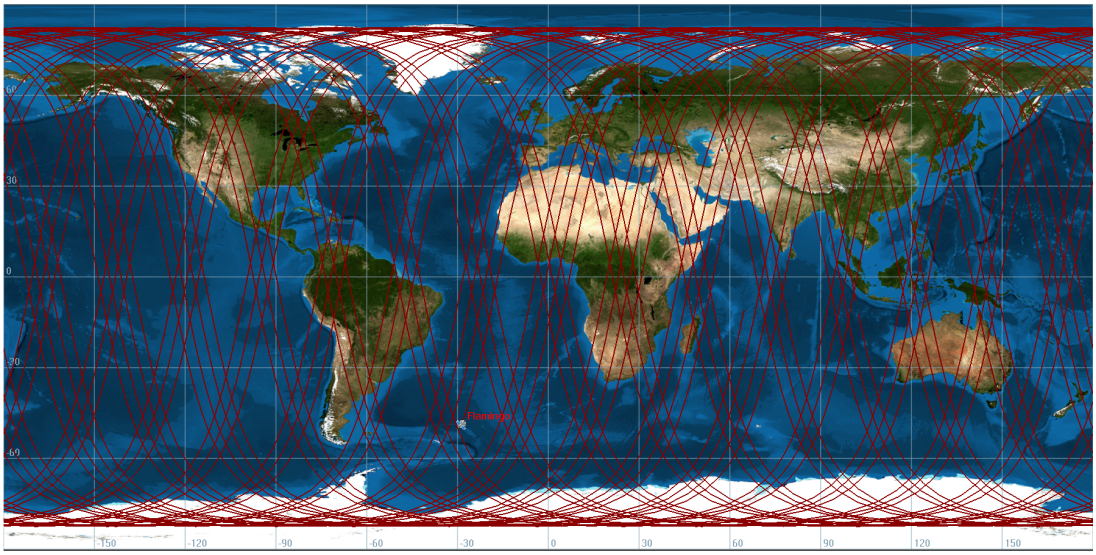

(b) Ground Track Representation

Figure 2.1: Representation of the orbit evolution

During this time period, no payload operation is considered, as the spacecraft is naturally propagating around the Earth, without any action from the propulsion subsystem. The orbit propagation for these first two months, along with the representation of the ground-track, is reported in Figure 2.1.
Setting the propagation time, the orbital parameters at the end of the this phase can be retrieved (Table 2.3).

Starting Epoch	**a** [km]	**e** [-]	**i** [°]	**Ω** [°]
18 Dec 2023 23:59:00	6890.417	97.396	0.00247	247.035

Table 2.3: Orbital Parameters after Commissioning

Such orbit presents a various amount of perturbations which may alter the nominal condition for the operation to occur, or, alternatively, that could allow us to exploit the change in certain orbital parameters for the purpose of the maneuver.

2.1. Orbit Perturbations

It is now worth to spend a few words on the environment in which the satellite will find itself during its lifetime. According to the orbit considered, the magnitude of the disturbance given by the different perturbations vary, resulting in a different change of the parameters considered. Not only the magnitude of the parameters can vary, but also the rate of change of the parameters. In fact, perturbations can manifest themselves with short-period, long-period or secular variations. The analysis of the major perturbations must then be performed along with their accurate modeling.

2.1.1. Gravity Gradient

The first of these perturbations to be considered is the gravity gradient, a perturbation caused by the non-uniformity of the Earth's gravitational field producing significant changes in some of the Keplerian elements.

The gravity gradient is defined in a mathematical way by means of a summation of components which can go as high as the order of accuracy that we want to consider. We know from the dynamics that the acceleration in an inertial frame is calculated as:

$$\mathbf{a} = \nabla U \tag{2.1}$$

The solution of the Laplace equation (2.2) provides the potential for a non spherical body

$$\nabla^2 U = 0 \tag{2.2}$$

The gradient of gravitational potential expressed in spherical coordinates is expressed as:

$$\nabla U = \frac{\partial U}{\partial r}\mathbf{u}_r + \frac{1}{r}\frac{\partial U}{\partial \phi}\mathbf{u}_\phi + \frac{1}{rcos\phi}\frac{\partial U}{\partial \lambda}\mathbf{u}_\lambda \tag{2.3}$$

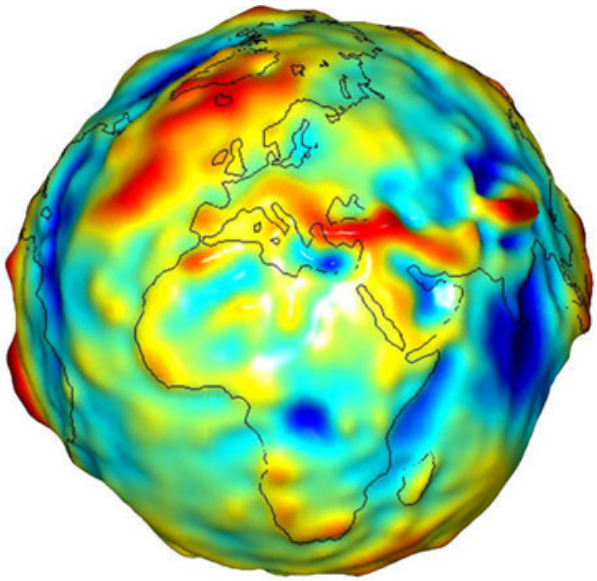

Figure 2.2: Earth's Gravity field

singularities arise when (r = 0) and $\phi = \pm 90$. The expression of the potential developed by Pines [7] avoids those singularities:

$$U = \frac{\mu}{r}\left(1 + \sum_{n=1}^{\infty}\left(\frac{R_{\otimes}}{r}\right)^{n}\sum_{m=0}^{n} A_{nm}(u)\left[C_{nm}cos(m\lambda)cos^{m}\phi + S_{nm}sin(m\lambda)cos^{m}\phi\right]\right) \tag{2.4}$$

This one can be then rewritten:

$$U = \frac{\mu}{r}\left(1 + \sum_{n=1}^{\infty}\left(\frac{R_{\otimes}}{r}\right)^{n}\sum_{m=0}^{n} A_{nm}(u)\left[C_{nm}r_{m}(s,t) + S_{nm}i_{m}(s,t)\right]\right) \tag{2.5}$$

where C_{nm} and S_{nm} are the gravitational coefficients, s, t, and u are given by

$$s = x/r, \quad t = y/r, \quad u = z/r = sin(\phi) \tag{2.6}$$

$r_m(s,t)$ and $i_m(s,t)$ are then computed with the recursive relationship

$$r_0 = 1, \quad r_1 = s, \quad i_0 = 0, \quad i_1 = t \tag{2.7}$$

$$r_m = s \cdot r_{m-1} - t \cdot i_{m-1}, \quad i_m = s \cdot i_{m-1} - t \cdot r_{m-1} \tag{2.8}$$

The coefficients $A_{nm}(u)$ are the derived Legendre functions (further derivations of the coeffiecients in [8]).
The trigonometric argument of the Legendre Polynomials constitutes surface Spherical

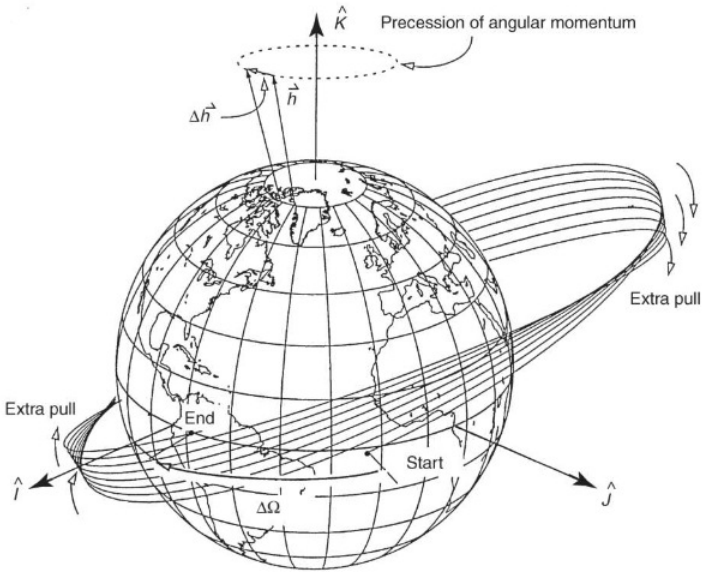

Figure 2.3: Westward Node Regression due to J_2 Effects

harmonics as they are periodic on the surface of a unit sphere. The magnitude of the zonal-harmonic effect suggests a physical interpretation to better understand its influence. The detailed analysis of the model exploited and the physical interpretation of the parameters, along with a further accurate derivation can be found in [9], [10]. A brief summary of the main implications will now be introduced.
The presence of secular effects caused by zonal harmonics has a simple physical explanation: the added attraction of the Earth's equatorial bulge introduces a force component toward the equator. Consequently, the resultant acceleration will cause the satellite to reach the the equator short of the crossing point for a spherical Earth. This phenomenon causes regression of the node (for direct orbits) or a counter rotation of the orbital plane around the polar axis.

Short-Periodic Effects from Zonal Harmonics Short-periodic variations cause oscillations in the elements with a fundamental period equal to the Keplerian period ($2\pi/n$). Excluding J_2, amplitudes of these oscillations are usually the smallest of all periodic contributions. J_2 produces effects for a near-Earth satellite position of the order of 8-10 km. The effect diminishes in terms of magnitude variation as the value of the altitude increases, reducing the effect to a km or two for GEO satellite. Other zonal harmonics also have an effect, even though it is much smaller, usually less than 50-100 m, which is way is often discarded or marginally considered.

Long-Periodic/Short-Periodic Beat Period from Zonal Harmonics This component of the motion is caused by the interaction of short-periodic and long-periodic variations. This interaction creates a beat period characterized by a high frequency oscillation with an amplitude that oscillates at the long-periodic frequency. The result is a high-frequency oscillation contained in a long periodic envelope. Magnitude of these contributions depend on time and vary from the size of the short-periodic variations up to the size of the long-periodic contributions. Remember that the SP variations are quite small, except for those due to J_2.

The feature that attracts us in particular is the secular change operated in the RAAN by the J_2 effects:

$$\dot{\Omega} = -\frac{3}{2} J_2 \sqrt{\frac{\mu}{a^3}} \left(\frac{R_e}{a} \right)^2 \cos i \tag{2.9}$$

The main point here is the dependence of this RAAN variation [4] with respect to the altitude. The more we raise the orbit, the higher the change in RAAN will be.
This is the crucial property on which the maneuver is based.

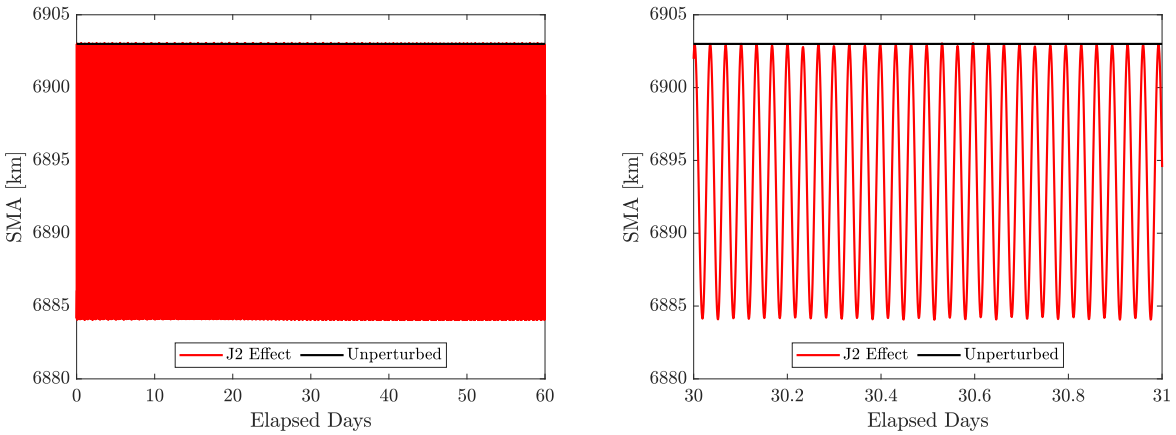

(a) Semi-major axis variation (60 days)

(b) Eccentricity variation (One day)

Figure 2.4: Variation of the semi major axis due to Gravity Gradient

[4] Smaller variations of the RAAN due to other types of perturbations are not considered

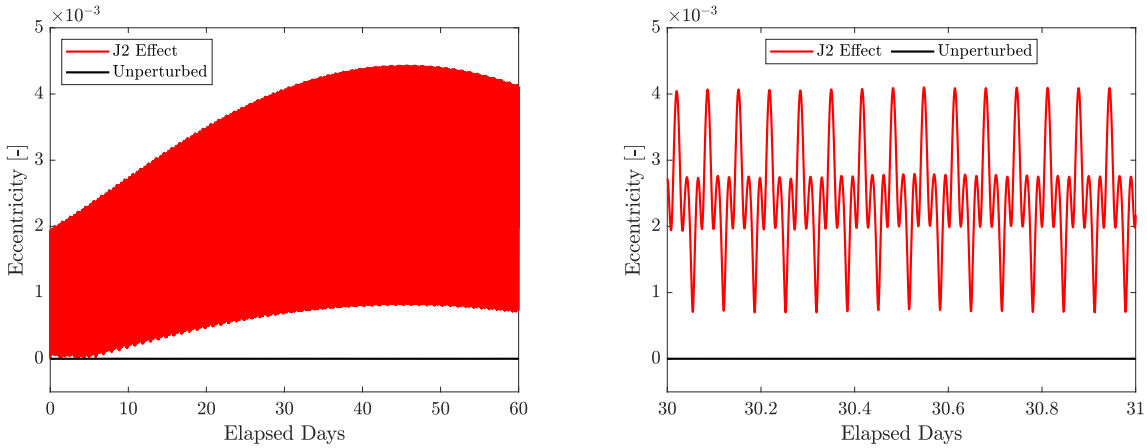

(a) Eccentricity variation (60 days) (b) Eccentricity variation (one day)

Figure 2.5: Variation of the eccentricity due to Gravity Gradient

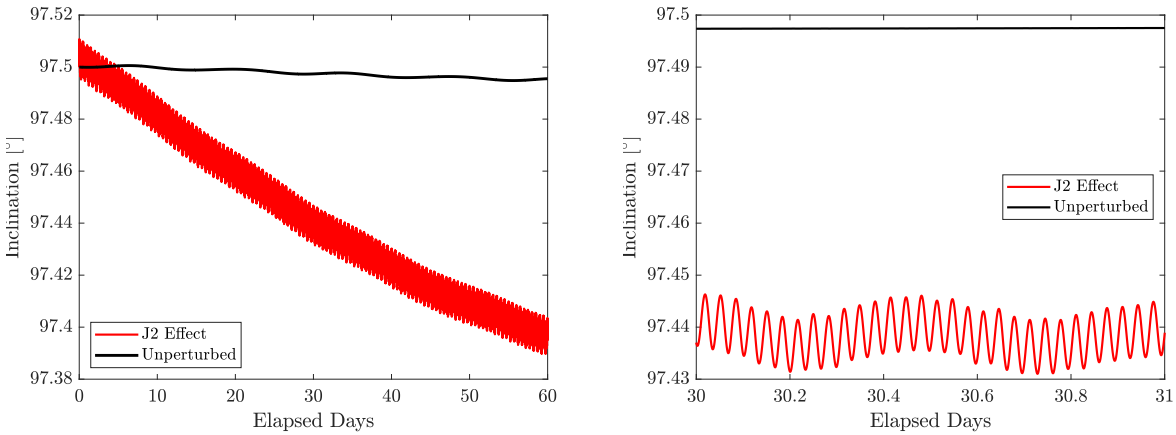

(a) Inclination variation (60 days) (b) Inclination variation (One day)

Figure 2.6: Variation of the inclination due to Gravity Gradient

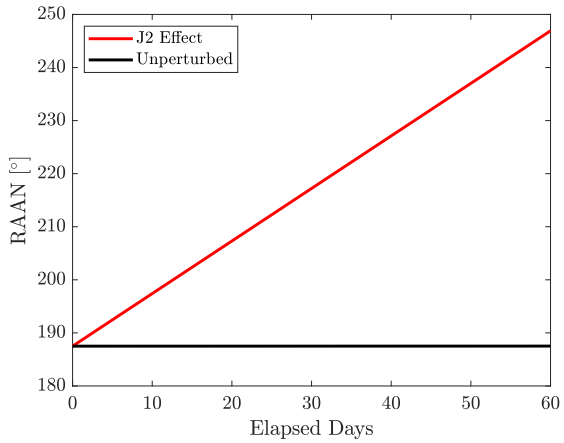

Figure 2.7: Variation of the RAAN due to Gravity Gradient

This peculiar property can be exploited in what are the so called Sun Synchronous Orbits (SSOs), aiming for a fixed orientation with respect to the Earth-Sun direction over time. Orbits parameters can be therefore tuned to allow a natural RAAN drift such that the satellite passes above the same point on the Earth at the same local solar hour, ensuring constant light condition.

2.1.2. Drag Effects

Aerodynamic drag, contrary to the natural RAAN drift induced by J_2, cannot be exploited for the purpose of the maneuver, as its main effect are only on the apogee lowering. However, since the orbit eccentricity is very low, it can be considered as an overall orbit altitude decrease, which in fact is of particular bother, as lowering the altitude the RAAN change will be different (and worse).
Nonetheless, given the orbit altitude, it is of major importance as it plays an important role in the change of orbit parameters, and its presence cannot be neglected.

$$\boldsymbol{a}_d = -\frac{1}{2}\rho v_{rel}^2 \frac{C_d A}{m_s}\hat{\boldsymbol{v}}_{rel} \tag{2.10}$$

$$\boldsymbol{v}_{rel} = \boldsymbol{v} - \boldsymbol{\omega}_{\otimes} \times \boldsymbol{r} + \boldsymbol{v}_w \tag{2.11}$$

and $\boldsymbol{\omega}_{\otimes}$ is the central bodies angular velocity vector, $\boldsymbol{w}$ is the local wind velocity, C_d is the drag coefficient, A is the cross sectional area normal to $\boldsymbol{v_{rel}}$, ρ is the atmospheric density, and m_s is the spacecraft mass.

The partial derivatives of the drag force with respect to position and velocity are:

$$\frac{\partial \boldsymbol{a}_d}{\partial \boldsymbol{r}} = -\frac{1}{2}\frac{C_d A}{m_s}\left(v_{rel}\boldsymbol{v}_{rel}\frac{\partial \rho}{\partial \boldsymbol{r}} + \rho \boldsymbol{v}_{rel}\hat{\boldsymbol{v}}_{rel}^T\left(\frac{\partial \boldsymbol{v}_w}{\partial \boldsymbol{r}} - \boldsymbol{\omega}_B^x\right) + \rho \boldsymbol{v}_{rel}\left(\frac{\partial \mathbf{v}_w}{\partial \boldsymbol{r}} - \boldsymbol{\omega}_B^x\right)\right) \tag{2.12}$$

$$\frac{\partial \boldsymbol{a}_d}{\partial \boldsymbol{v}} = -\frac{1}{2}\frac{C_d A}{m_s}\left(\boldsymbol{v}_{rel}\hat{\boldsymbol{v}}_{rel}^T + v_{rel}\boldsymbol{I}_3\right) \tag{2.13}$$

As the effect of this perturbation is based on the density, depending on the level of accuracy required (depending on the altitude of the s/c for a start), a model of the atmosphere shall be provided. The Jacchia Roberts model ([11]) embedded in the GMAT software

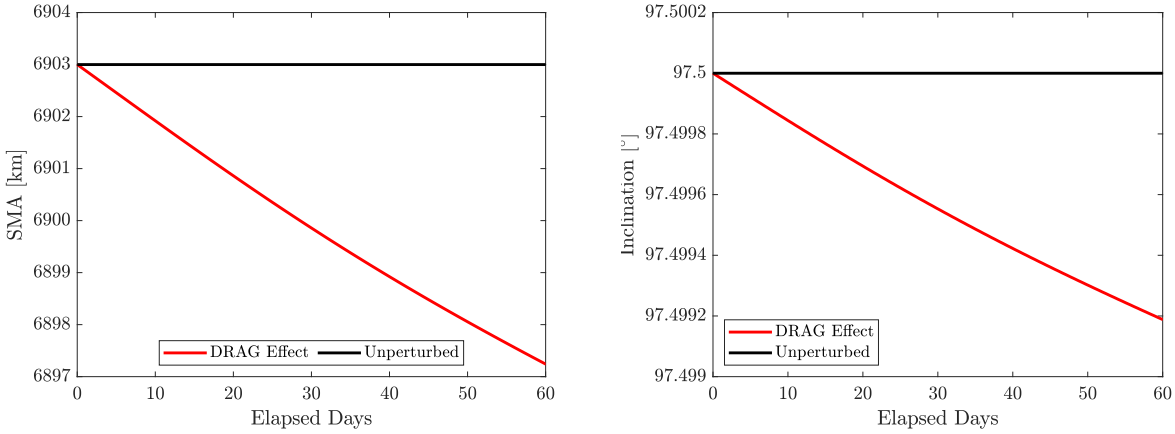

(a) SMA Decay (b) Inclination variation

Figure 2.8: Variation of the SMA and inclination for a spacecraft subject to drag resistance

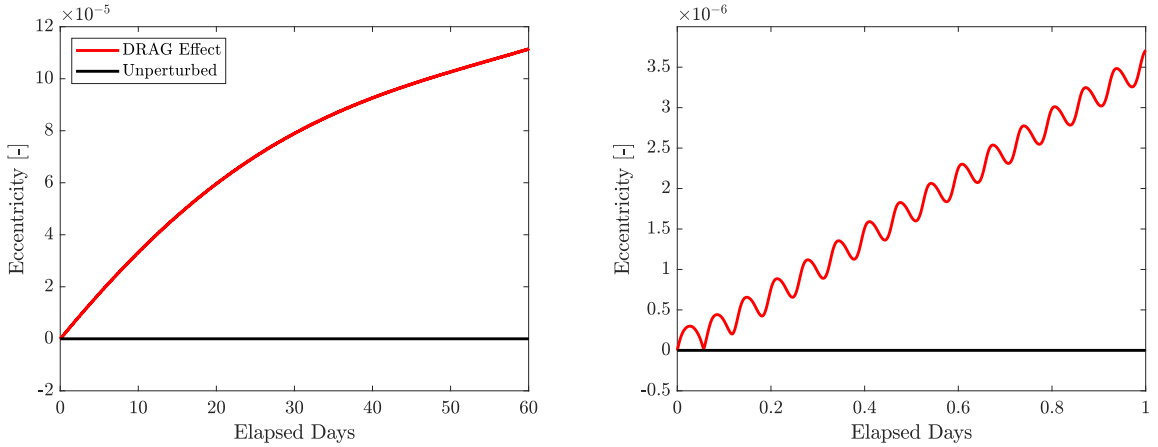

(a) Eccentricity variation (60 days) (b) Eccentricity Variation (one day)

Figure 2.9: Variation of the eccentricity due to drag resistance

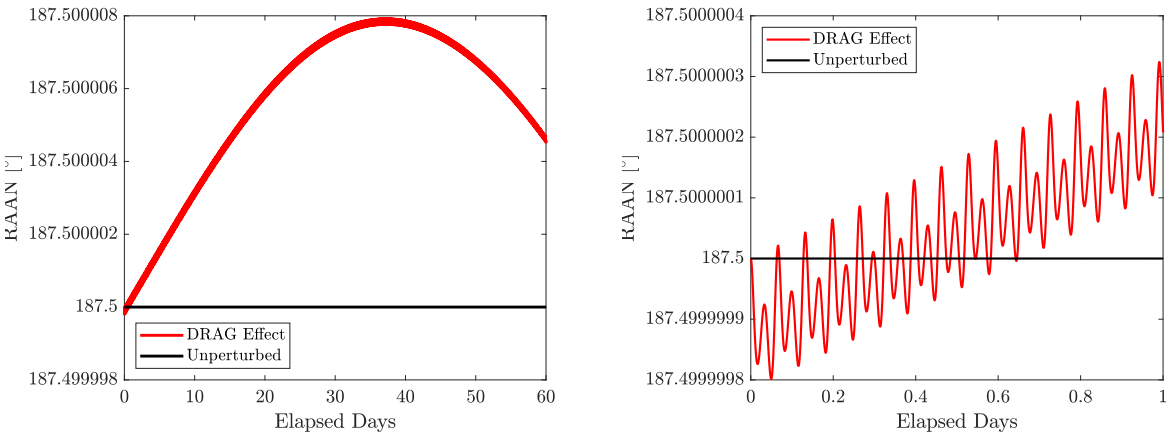

(a) RAAN variation (60 days) (b) RAAN variation (one day)

Figure 2.10: Variation of the RAAN due to drag resistance

will be used for this purpose, allowing to define densities up to 2500 km of altitude (see Appendix B). The model also includes latitudinal, seasonal, geomagnetic, and solar effects on the density, allowing a robust drag considerations.

2.2. Eclipse Considerations

The transit of a spacecraft through the Earth's shadow presents an additional challenge due to the high power demands of electric propulsion engines, which can hinder their usage.

Nonetheless, some on-board instruments may be affected by the sun presence, which may corrupt their functionality if not well accounted. Some considerations can be made also from the thermal point of view, examining the sunlight period during the maneuver and provide a correct pointing for the thermal and optic management, but that's beyond the scope of the work. The major implication that we're interested in is the discontinuous thrust effect given by these events. This can cause, even if very small, changes in the eccentricity of the orbit, which will tend to increase, with the apogee laying in the shadow arc. That's why the introduction of Eclipse in our discussion is mandatory.

[12] The computation of the eclipse region is implemented through the Montebruck and Gill [13] analysis (more detailed model on shadow geometry in [14])

$$\boldsymbol{r}_{\odot/sc} = \boldsymbol{r}_{\odot} - \boldsymbol{r}_{sc} \tag{2.14}$$

$$\boldsymbol{r}_{B/sc} = \boldsymbol{r}_{B} - \boldsymbol{r}_{sc} \tag{2.15}$$

where $\boldsymbol{r}_{\odot}$ indicates the sun vector, $\boldsymbol{r}_{sc}$ indicates the spacecraft vector and $\boldsymbol{r}_{B}$ is the .... vector.
We can define then the following quantities:

$$a_{SR} = arcsin\left(\frac{\boldsymbol{r}_{\odot}}{||\boldsymbol{r}_{\odot/sc}}\right) \tag{2.16}$$

$$a_{BR} = arcsin\left(\frac{\boldsymbol{r}_{B}}{||\boldsymbol{r}_{B/sc}}\right) \tag{2.17}$$

$$a_{D} = arccos\left(\frac{\boldsymbol{r}_{B/sc}\boldsymbol{r}_{\odot/sc}}{||\boldsymbol{r}_{B/sc}||\ ||\boldsymbol{r}_{\odot/sc}||}\right) \tag{2.18}$$

$$a_{SR} + a_{BR} > a_{D} \tag{2.19}$$

The sunlight fraction is a discontinuous function of the geometry of spacecraft, Sun, and occulting body positions

$$\gamma = \begin{cases} 0, & a_{SR} + a_{BR} > a_{D}\ \&\ \ a_{SR} \leq a_{BR} \\ (0,1), & a_{SR} + a_{BR} > a_{D}\ \&\ \ a_{SR} > a_{BR} \\ 1, & a_{SR} + a_{BR} \leq a_{D} \end{cases} \tag{2.20}$$

where the total eclipse occurs in umbra, and in the intermediate case is itself a discontinuous function that depends on if the spacecraft is in penumbra or antumbra.
Additional relations from the overlapping disc geometry allow for the computation of the sunlight fraction in each of these cases [15]. However, zero thrust constraint is enforced in the case of both partial and total eclipse, given the model adopted. It is important, to reduce the change in eccentricity and other possible deviations so the thrust is considered symmetrical with respect to the orbit.
The AoL at the eclipse center (θ_C) is calculate at each time step of the propagation. Thrust is therefore turned off for a symmetric fraction where

$$\theta_C - 2\pi\frac{1-DC}{4} \leq \theta \leq \theta_C + 2\pi\frac{1-DC}{4} \tag{2.21}$$

the same consideration is valid for the point opposite to θ_C in the orbit.

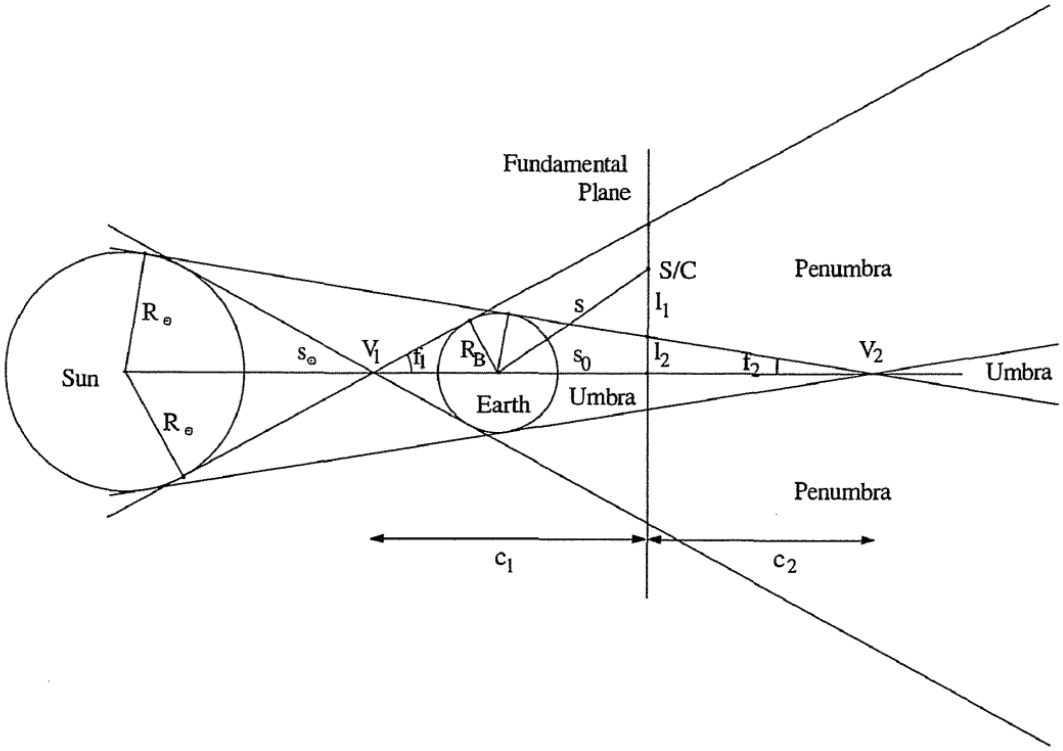

Figure 2.11: Eclipse model

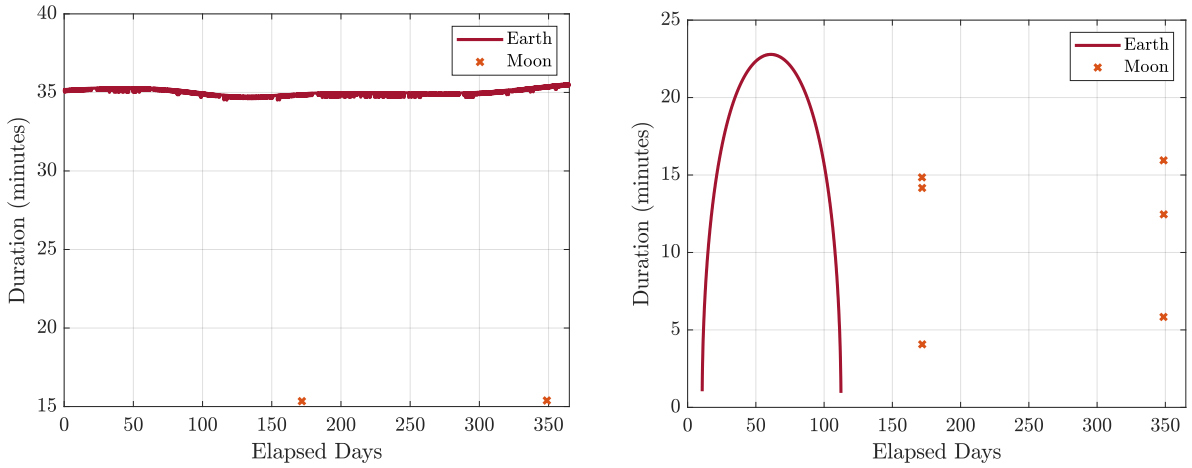

(a) Eclipse events in the 10:30 A.M. orbit (b) Eclipse events in the 6 A.M. orbit

Figure 2.12: Eclipse Durations difference for the different orbit

2.2.1. Solar Radiation Pressure

Solar radiation pressure (SRP) is a physical phenomenon that occurs when photons from the sun collide with a spacecraft's surface, resulting in a transfer of momentum. This transfer of momentum can cause a small but significant force on the spacecraft, which can affect its trajectory and orbit.
There are several approaches to modeling SRP, including empirical, analytical, and numerical methods [16], [17]. Empirical models rely on experimental data and can provide accurate results, but may not be suitable for all spacecraft configurations. Analytical methods use mathematical models to estimate SRP and can provide quick and efficient results, but may not be as accurate as numerical methods.

$$\boldsymbol{a}_{SRP} = \nu P_s r_{AU}^2 \frac{C_r A}{m} \frac{\boldsymbol{r}_{vs}}{r_{vs}^3} \tag{2.22}$$

where, $r_{vs} = r - r_s$ is the Sun-Spacecraft vector, r is the position of the spacecraft in inertial coordinates, r_s is the position of the Sun in inertial coordinates, r_{AU} is the Sun-Earth distance, m is the spacecraft mass, A is the spacecraft area, P_s is the solar flux at 1 AU and C_r is the reflectivity coefficient.

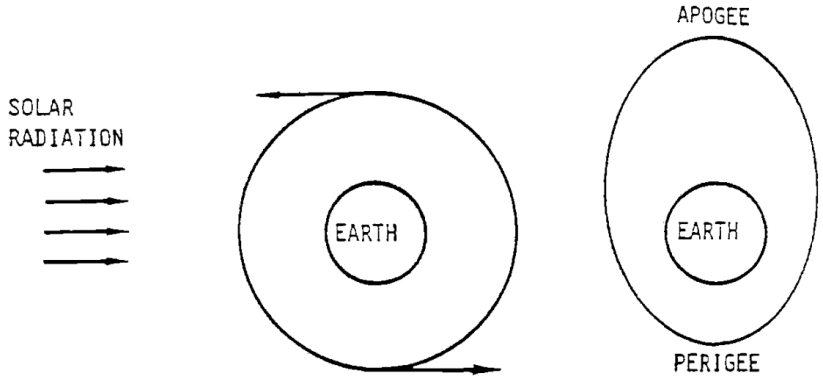

Figure 2.13: Eccentricity change due to SRP

ν is instead the eclipse factor [5] defined as

$$\nu = \left(1 - \frac{\gamma}{100}\right) \tag{2.23}$$

Solar Radiation Pressure is highly dependant on spacecraft geometry and properties, as

[5]The percent Shadow γ is defined in 2.20, for a complete derivation of the percent shadow partial derivatives see [8]

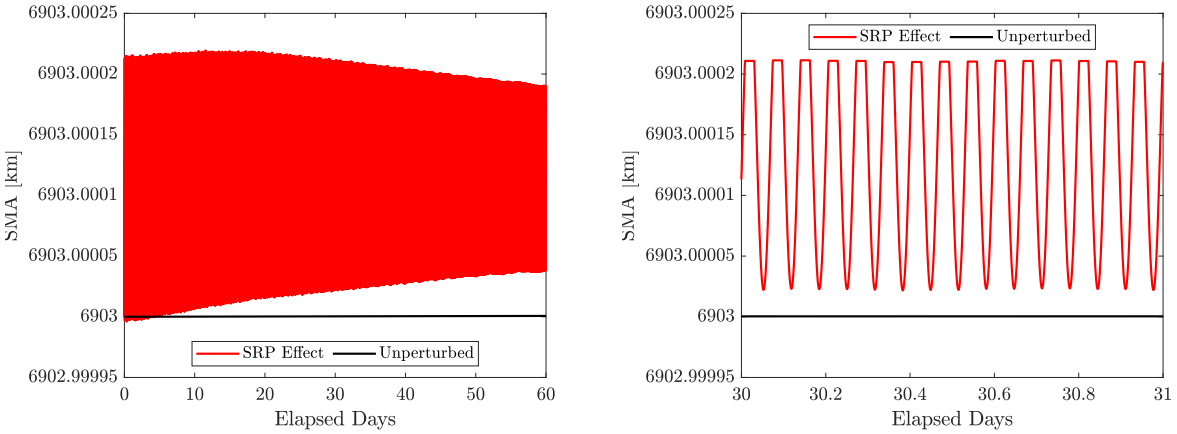

(a) Semi-major axis variation (60 days) (b) Semi-major axis variation (One day)

Figure 2.14: Inclination variation

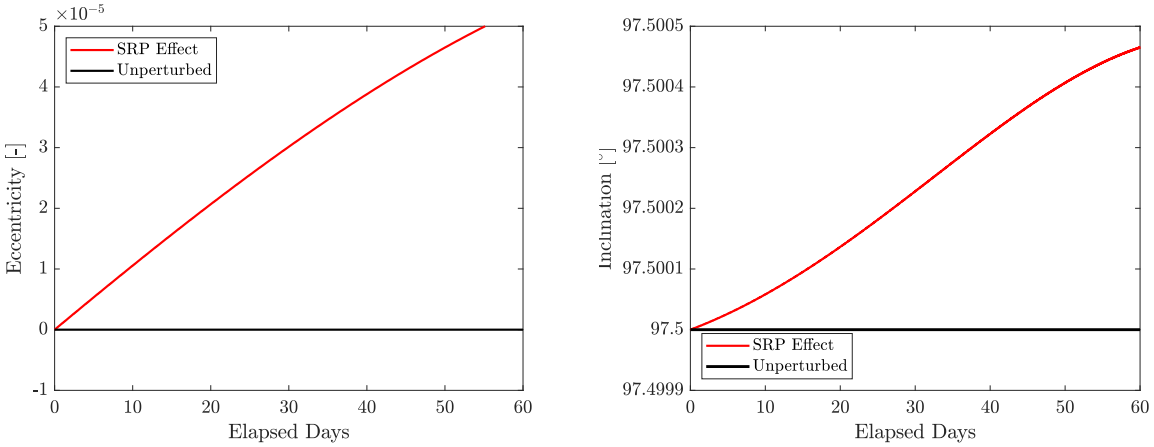

(a) Eccentricity variation (b) Inclination variation

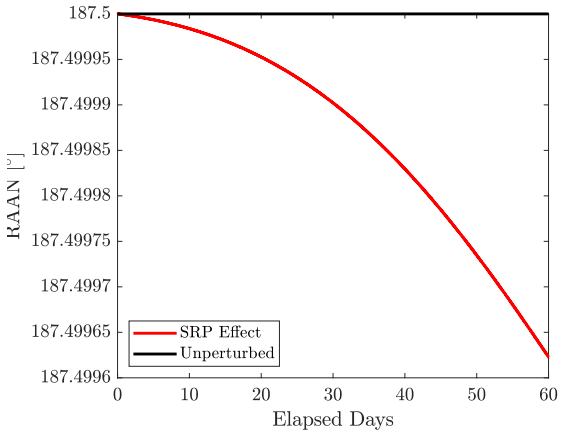

(c) RAAN variation

Figure 2.15: Variation of keplerian elements due to SRP

well as its attitude. The relative orientation between high surfaces can modify the momentum exchange between the solar particles and the satellite. However, as the magnitude change is relatively small with respect to other perturbations, and due to the fact that in this dissertation attitude considerations are disregarded, it is not necessary to have a accurate modeling [6] of the SRP.

[6]Preliminary model reported is taken from [9], but more detailed analysis can be found in [13], [18]

3 | State of the Art

3.1. Overview of Low-Thrust Spacecraft Manoeuvres

Low-thrust transfer orbits have been an increasingly popular trend in the latest years due to their high efficiency and versatility [19]. Unlike traditional chemical propulsion systems, which require a large amount of propellant to achieve significant changes in velocity, low-thrust propulsion systems can generate continuous thrust over long periods of time to produce the required velocity change. This enables spacecraft to reach their target destinations with less propellant, lower launch costs, and a greater degree of mission flexibility. In this context, some analyses[1] have been carried out to exploit the best analytical and numerically integrated solution to the low-thrust transfer problem.

3.1.1. Edelbaum Transfer

The classic guideline used to compute the optimal condition for the transfer between two co-planar circular orbits has been proposed by Edelbaum in his paper [21], providing a very reliable tool to compute the transfer cost and its parameters.
The base of his work has been adopted in many analysis to improve the efficiency of the maneuver, but mostly to provide a tool to be used in a wide range of applications, which may consider a lot of particular conditions depending on the mission.
Edelbaum's seminal work, in fact, is mainly to be considered as a preliminary evaluation, having to be refined and specialized for the application.
The analysis deals with a wide range of maneuvers, spanning from high to low thrust and considering different magnitude changes in the orbital parameters. In particular, the variation of the latter can be expressed as a function of the α angle, formed by the velocity vector and the in-plane thrust vector component, and the β angle, formed by the velocity vector and the out-of-plane thrust vector component. Some considerations, in fact, regarding the properties of the orbit were made, simplifying the problem of the optimal solution search. Its original analysis consider small changes in orbital elements allowing a linear model for the equations. The linearized set of Gauss Planetary equations

[1] General analysis of Low-Thrust Orbital Maneuvers in [20]

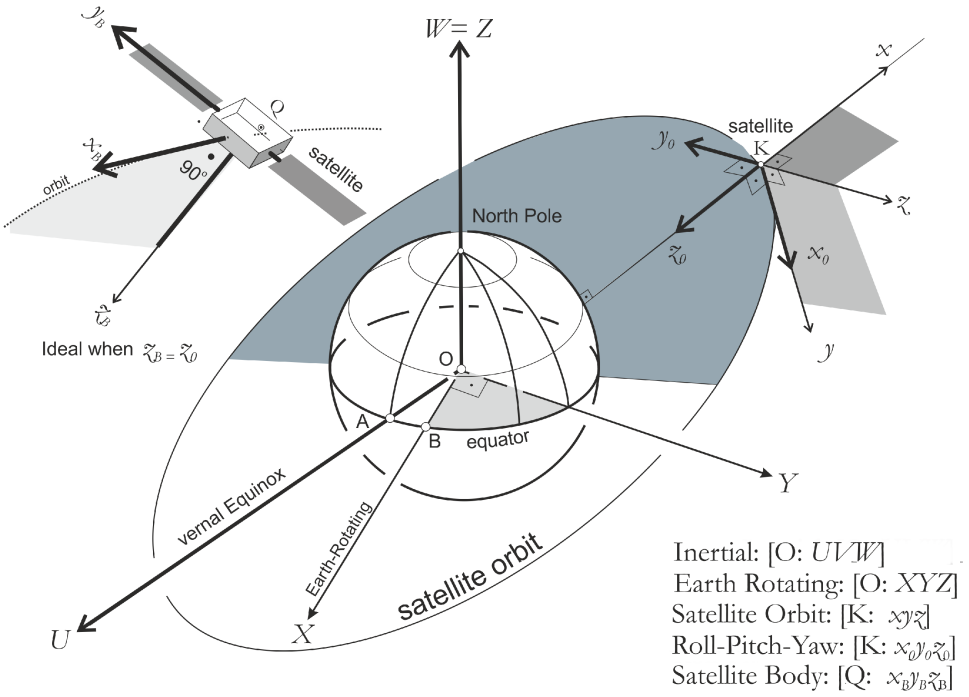

Figure 3.1: Frames of reference

is here reported:

$$\frac{da}{dt} = \frac{2a}{V_0}\frac{F_T}{m} \tag{3.1}$$

$$\frac{de}{dt} = \frac{2cos\theta}{V_0}\frac{F_T}{m} + \frac{2sin\theta}{V_0}\frac{F_N}{m} \tag{3.2}$$

$$\frac{di}{dt} = \frac{cos\,(\omega+\theta)}{V_0}\frac{F_z}{m} \tag{3.3}$$

$$\frac{d\Omega}{dt} = \frac{sin\,(\omega+\theta)}{iV_0}\frac{F_z}{m} \tag{3.4}$$

$$\frac{d\omega}{dt} = \frac{2sin\theta}{eV_0}\frac{F_T}{m} + \frac{cos\theta}{eV_0}\frac{F_N}{m} - \frac{sin\,(\omega+\theta)}{iV_0}\frac{F_z}{m} \tag{3.5}$$

where:

$$F_t = Fcos(\beta)cos(\alpha) \tag{3.6}$$

$$F_n = Fcos(\beta)sin(\alpha) \tag{3.7}$$

$$F_h = Fsin(\beta) \tag{3.8}$$

The optimum steering analysis carried out by Edelbaum implied the following assumptions:

- Averaging of the orbital dynamics over one period.
- Orbits remain circular during transfer.
- Thrust yaw angle is kept constant during each revolution, but it changes from one revolution to another
- The sign switch of the yaw angle is performed at the nodes of the transfer orbit.

Another important condition, given the consideration about the low-thrust maneuver, is that the acceleration in any of the three direction shall be much smaller than the gravitational acceleration ($a << \mu/r^2$).
Given this simplified model, the equations of motion above reduce to:

$$\dot{a} = \frac{2af_t}{V} \tag{3.9}$$

$$\dot{i} = \frac{f_h cos\alpha}{V} \tag{3.10}$$

$$\dot{\Omega} = \frac{f_h sin\alpha}{V sin(i)} \tag{3.11}$$

$$\dot{\alpha} = n - \frac{f_h sin\alpha}{V tan(i)} \tag{3.12}$$

$$\tag{3.13}$$

The transfer exploiting the yaw switch steering at the antinodes [22] can be visualized in Figure 3.2
As the angle β is held piece-wise constant during revolutions some contributions can be eliminated in the equations above, leaving us with a set of differential equations:

$$\dot{a} = \frac{2af_t}{V} \tag{3.14}$$

$$\dot{i} = \frac{f_h cos\theta}{V} \tag{3.15}$$

$$\dot{\theta} = n \tag{3.16}$$

$$\tag{3.17}$$

Angular position can be now averaged out, integrating with respect to θ, holding β, V, and f constant

$$\int_0^{2\pi} \frac{di}{dt} d\theta = \frac{2f sin(\beta)}{V} \int_{-\pi/2}^{pi/2} cos(\theta) d\theta \tag{3.18}$$

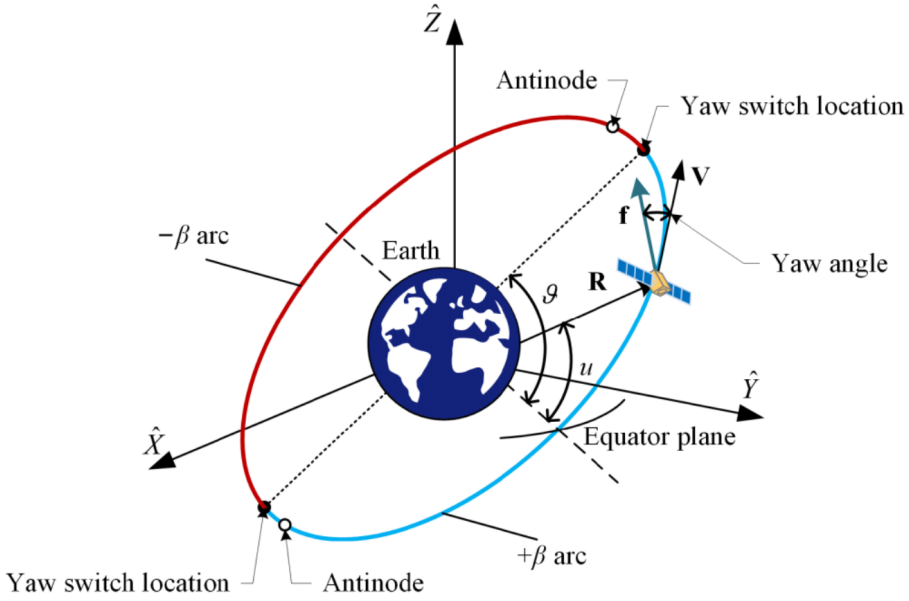

Figure 3.2: Edelbaum Transfer Design

Computing the integral and rearranging the equation, the velocity variation over time can be expressed as:

$$\frac{di}{dt} = \frac{2}{\pi}\frac{fsin(\beta)}{V} \tag{3.19}$$

From 3.1, combining the relation of the semi major axis with the velocity, variation of the velocity with time can be obtained:

$$\frac{dV}{dt} = -fcos(\beta) \tag{3.20}$$

The analysis of the optimal condition in terms of the steering angle β will now be conducted. In particular, the functional to maximize $\mathcal{I}$ is computed:

$$\mathcal{I} = \int_{V_0}^{V_f} \frac{di}{dV} dV \tag{3.21}$$

Let us now then represent the variation of the inclination with the velocity

$$\frac{di}{dt} = \frac{di}{dV}\frac{dV}{dt} = \frac{2}{\pi}\frac{fsin(\beta)}{V} \tag{3.22}$$

holding, respectively:

$$\frac{di}{dV}(-fcos(\beta)) = \frac{2fsen(\beta)}{\pi V} \quad \rightarrow \quad \frac{di}{dV} = -\frac{2tan(\beta)}{\pi V} \tag{3.23}$$

Let us now adjoin the functional $\mathcal{I}$ with the constraint integral $\mathcal{J}$ defined as:

$$\mathcal{J} = \int_{V_0}^{V_f} \left(\frac{dt}{dV} \right) dV = const \tag{3.24}$$

The augmented Integral can now be written as:

$$\mathcal{K} = \mathcal{I} + \lambda \mathcal{J} = \int_{V_0}^{V_f} \left(-\frac{2}{\pi V} tan(\beta) - \frac{-\lambda}{f cos(\beta)} \right) dV \tag{3.25}$$

The necessary condition for the stationary solution

$$\frac{\partial}{\partial \beta} \left(-\frac{2}{\pi V} tan(\beta) - \frac{-\lambda}{f cos(\beta)} \right) = 0 \tag{3.26}$$

The optimal steering law is then retrieved:

$$V sin\beta = V_0 sin\beta_0 \tag{3.27}$$

As the thrust acceleration is assumed to be constant, the minimization of the ΔV translates to the minimization of the transfer time t:

$$\Delta V = ft \tag{3.28}$$

The functional I and the integral constraint J can be mutually interchanged to yield

$$\frac{\partial}{\partial \beta} \left(\frac{1}{f cos(\beta)} \lambda_i \frac{2}{\pi V} tan(\beta) \right) = 0 \tag{3.29}$$

λ then is computed:

$$\lambda = -\frac{2f}{\pi V_0 sin(\beta_0)} \tag{3.30}$$

The variation of the velocity with the time utilizing the expression of the of the optimal steering law β is then retrieved:

$$\frac{dV}{dt} = -f cos(\beta) \quad \rightarrow \quad f dt = -\frac{dV}{cos(\beta)} \tag{3.31}$$

Integrating the last equation and rearranging we find

$$\Delta V = V_0 cos(\beta_0) - V cos(\beta) \quad \rightarrow \quad V^2 = V_0^2 + \Delta V^2 - 2 \Delta V V_0 cos(\beta_0) \tag{3.32}$$

In the same way the inclination variation is computed:

$$\frac{di}{dV} = -\frac{2}{\pi V} tan(\beta) \quad \rightarrow \quad di = -\frac{2}{\pi V} tan(\beta) \tag{3.33}$$

where V is retrieved from $V sin(\beta) = V_0 sin(\beta_0)$. The final formulation is

$$\Delta i = -\frac{2}{\pi}\beta_0 + \frac{2}{\pi} sin^{-1}\left(\frac{V_0 sin(\beta_0)}{V}\right) \tag{3.34}$$

However, the inverse sine term yields a double-value in the $(0, 2\pi)$, so a differentiation is necessary to distinguish the values. In particular:

$$\text{If} \quad sin^{-1}\left(\frac{V_0 sin(\beta_0)}{V}\right) < \frac{\pi}{2} \quad \rightarrow \quad sin^{-1}\left(\frac{V_0 sin(\beta_0)}{V}\right) \tag{3.35}$$

$$\text{If} \quad sin^{-1}\left(\frac{V_0 sin(\beta_0)}{V}\right) > \frac{\pi}{2} \quad \rightarrow \quad \pi - sin^{-1}\left(\frac{V_0 sin(\beta_0)}{V}\right) \tag{3.36}$$

The inclination variation can be now defined[2] as a function of the β angle value:

$$\text{If} \quad \beta < \frac{\pi}{2} \quad \rightarrow \quad \Delta i = \frac{2}{\pi}(\beta - \beta_0) \tag{3.37}$$

$$\text{If} \quad \beta > \frac{\pi}{2} \quad \rightarrow \quad \Delta i = 2 - \frac{2}{\pi}(\beta + \beta_0) \tag{3.38}$$

As the transfer considered is based on the use of a low thrust propulsion system, many revolutions will be needed to achieve the final target orbit. This kind of approach has been widely used from LEO to GEO transfers [23]to purely changes in inclination or eccentricity. The transfer has been also combined with other approaches such as gravity assists and multiple gravity assists to further reduce the propellant consumption and increase the mission flexibility.

However, despite its many advantages, the Edelbaum transfer is not free from limitations. One of the major ones is its sensitivity to perturbations, such as variations in the gravity field, atmospheric drag, and solar radiation pressure, meaning that not considering such kind of perturbations implies a not so accurate analysis as the additional change of the parameters brought by the modified dynamics. As a result, accurate modeling of these perturbations is essential for achieving the desired trajectory and possibly reducing the propellant consumption.

In addition, the assumption of circularity of the orbits, requires sometimes to be relaxed (as the thrust phase can modify the eccentricity value during the maneuver), so the necessity to construct a robust tool is needed to define as precisely as we can the problem

[2]The value 2 in Equation 3.38 is the value in radians (114.6 °)

that has to be faced. Representation of the maneuver sequence [24]is in Figure 3.3.

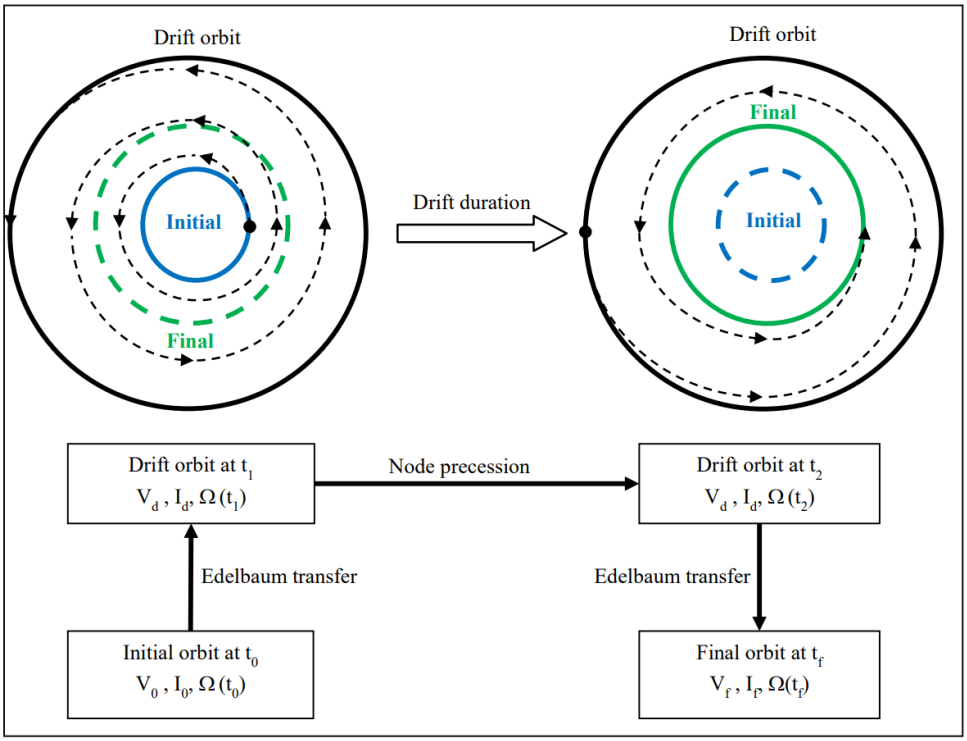

Figure 3.3: Split Edelbaum Sequence representation

3.1.2. Kechichian extension of the Edelbaum transfer

As above stated, the Edelbaum work providing the optimal steering law for transfers between inclined circular orbits is very reliable, and it has been widely used as a preliminary analysis for low-thrust maneuvers. But some integration to provide a better and robust formulation have been introduced.

The extension introduced by Kechichian [25] consists in the reformulation of the Edelbaum low thrust transfer problem using Optimal Control theory (different formulation with a direct approach found in [26]). The considered time-optimal problem involves a series of low-thrust velocity changes that are applied over a period of time to gradually adjust the spacecraft's trajectory from the elliptical orbit to the circular orbit. The transfer problem is now formulated in a slightly different way, recasted as a time minimum problem, given initial (V_0, i_0) and final parameters (V_f, i_f).

Let the performance index be defined in the way:

$$\mathcal{J} = \int_{t_0}^{t_f} \mathcal{L} dt \tag{3.39}$$

$\mathcal{L}$, in the case of the time minimum problem is equal to 1.
We consider the variational Hamiltonian $\mathcal{H}$[3]

$$\mathcal{H} = 1 + \lambda_i \left(\frac{2f}{\pi V} sin(\beta) \right) + \lambda_V \left(-f cos(\beta) \right) \tag{3.40}$$

and the Euler-Lagrange equations:

$$\dot{\lambda}_V = -\frac{\partial \mathcal{H}}{\partial V} = \frac{2f sin(\beta)}{\pi V^2} \lambda_i \tag{3.41}$$

$$\dot{\lambda}_i = -\frac{\partial \mathcal{H}}{\partial i} = 0 \tag{3.42}$$

Of course, optimality condition is reached with the stationarity of the Hamiltionian, given by:

$$\frac{\partial \mathcal{H}}{\partial \beta} = \lambda_i \frac{2f}{\pi V} cos(\beta) + f \lambda_V sin(\beta) = 0 \tag{3.43}$$

which yields:

$$tan(\beta) = -\frac{2\lambda_i}{\pi V \lambda_V} \tag{3.44}$$

thus:

$$\mathcal{H} = 0 = 1 + \frac{2f}{\pi V} sin(\beta) \lambda_i - f cos(\beta) \lambda_V \tag{3.45}$$

$$\frac{\partial \mathcal{H}}{\partial \beta} = 0 = \frac{2f}{\pi V} sin(\beta) \lambda_i + f sin(\beta) \lambda_V \tag{3.46}$$

Resulting in

$$\lambda_i = -\frac{\pi sin(\beta) V}{2f} = \text{const} \tag{3.47}$$

$$\lambda_V = \frac{cos(\beta)}{f} \tag{3.48}$$

Integrating:

$$f dt = -\frac{dV}{cos(\beta)} = \frac{-dV}{\pm \left(1 - sin^2(\beta)\right)^{1/2}} \tag{3.49}$$

$$f \int_0^t dt = -\int_{V_0}^{V} \frac{V dV}{\pm \left(V^2 - V_0^2 sin^2(\beta_0)\right)^{1/2}} \tag{3.50}$$

[3]Further Analysis in [27], [28]

An expression of tan(β) has to be derived. Starting from the differentiation of Equation 3.44 using Equation 3.41, Equation 3.42, we arrive at the formulation of the control law, wirtten in the form of the tan(β):

$$tan(\beta) = \frac{V_0 sin(\beta_0)}{V_0 cos(\beta_0) - ft} \tag{3.51}$$

Combining this with 3.50

$$V = \left(V_0^2 + f^2 t^2 - 2V_0 cos(\beta_0 ft)\right)^{1/2} \tag{3.52}$$

Time history and total inclination change can be retrieved:

$$\Delta i = \frac{2}{\pi}\left[tan^{-1}\left(\frac{ft - V_0 cos(\beta_0)}{V_0 sin(\beta_0)}\right) + \frac{\pi}{2} - \beta_0\right] \tag{3.53}$$

3.1.3. Low-Thrust with Earth-Shadow Eclipses

A further extension of the analysis is provided by Kluever, in his paper, considering also Earth shadow eclipses causing mainly discontinuous thrust in the case of solar electric propulsion, accounting therefore for an accurate modeling of the transfer.
In this case, since the thrust time will be clearly less than the continuous thrust analysis, we do not expect a better performance in terms of transfer time[4]. But, as he demonstrates, the continuous and discontinuous thrust case hold very similar profiles in terms of state trajectories.
Starting from the equation of the velocity $\Delta V = ft$, we can rewrite it as a discrete component of the analysis:

$$\Delta V_{k+1} = \Delta V_k + f\Delta t; \qquad k = 0, 1, 2, ..., N \tag{3.54}$$

where

$$t_{k+1} = t_k + \frac{(\Delta V_{k+1} - \Delta V_k)}{f}; \qquad k = 0, 1, 2, ..., N \tag{3.55}$$

The two major constraints introduced are now:

- Spacecraft mass decrease
- Discontinuous thrust profile

[4]Formulation of a minimum-time optimization in [29], [30]

Therefore the changing term in the equation above is the thrust acceleration f (T/m), which has to be rewritten as:

$$t_{k+1} = t_k + \frac{(\Delta V_{k+1} - \Delta V_k)}{\bar{f}_k w_k} \tag{3.56}$$

The weighting w_k is function of the Earth shadow angle $\Delta\theta_{SH}$:

$$w = 1 - \frac{\Delta\theta_{SH}}{2\pi} \tag{3.57}$$

In particular, a value of $w = 1$ implies a continuous thrust profile, meaning that the spacecraft is entirely in sunlight during the whole revolution, whereas $0 < w < 1$ indicates a penumbra condition.

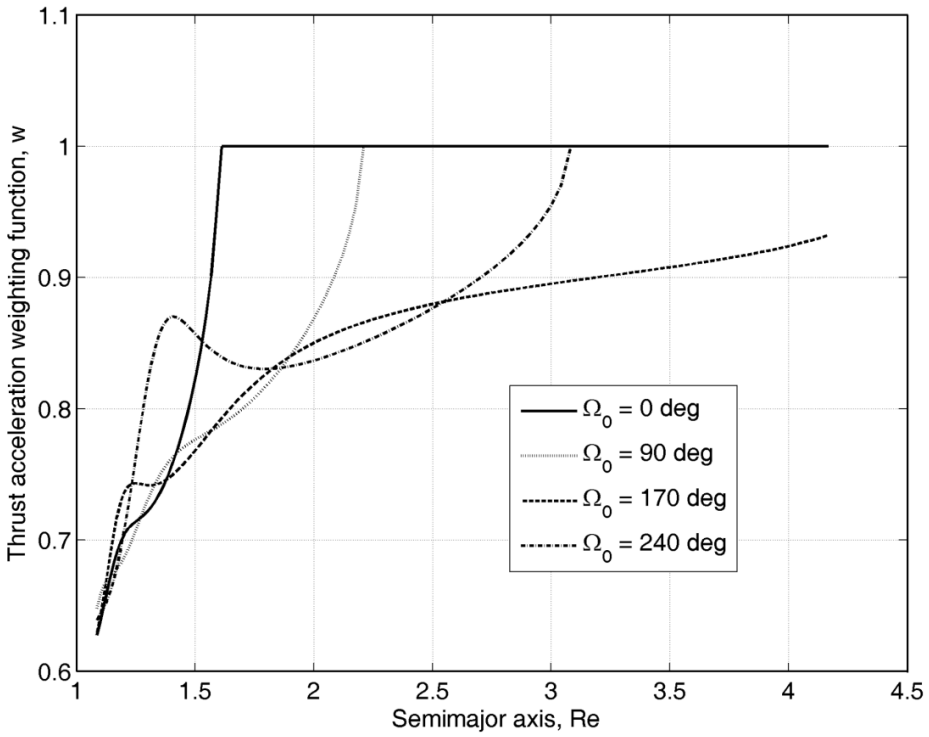

Figure 3.4: Example of the weighting function change during a LEO-GPS transfer

To summarize the procedure exploited, given the initial and target circular orbit radii, inclination change, and initial thrust acceleration f_0, computation of the total ΔV and transfer time t_f of the Edelbaum's solution for the continuous-thrust case.
The continuous-transfer time t_f is then divided into N segments, where the discrete histories for V_k, a_k, and i_k can be retrieved.

along with the knowledge of the departure date and initial orbital elements, the position of the Sun with respect to the spacecraft can be computed, and with it the Earth shadow arc can be computed, by employing the average thrust acceleration and assigning the correspondent weight in the three different possibilities.
Finally, propagate the ascending node angle ahead in time using equations computing the natural RAAN drift and the simple first order expansion to compute the RAAN value of the next segments. The recursive equations are repeated until all N segments of Edelbaum's solution have been processed.
As the simplification of the transfer still implies the fact that the orbits remain circular during each revolution, this may result in non accurate solution, but as the numerical solutions of the equations provided by the Kluver analysis states that the eccentricity doesn't exceed the 0.1 value, the preliminary analysis conducted is reliable.
But ultimately, the solution provided by Edelbaum integrated with the Kechichian optimal control theory and considering eclipse events, is not to be intended as an accurate solution, but as a fast algorithm not requiring a numerical integration.
More accurate solutions will consider various thrust profile changes or either various thrust magnitude changes. Eccentricity constraints should also be relaxed, as difference in apogee and perigee may play an important role [31].

3.2. Review of Optimization Techniques

3.2.1. Optimal Control Problem

Consider a dynamical system of n first-order differential equations

$$\dot{\mathbf{x}}(t) = \mathbf{f}(\mathbf{x}(t), \mathbf{u}(t), t) \tag{3.58}$$

where $\mathbf{x}(t) = [x_1(t), x_2(t), ..., x_n(t)]^T$ is the state vector and $\mathbf{u}(t) = [u_1(t), u_2(t), ..., x_r(t)]^T$ is the control variables vector.
The formulation of the optimal control problem is to find the r control function such that they minimize a certain objective function ([32], [33]) defined as

$$J = \phi(x(t_f), t_f) + \int_{t_0}^{t_f} L(\mathbf{x}(t), \mathbf{u}(t), t)dt \tag{3.59}$$

The scalar J is called a functional as it maps functions, specifically the path $\boldsymbol{x}$ and the control $\boldsymbol{u}$, into a scalar number. However, generally, we refer to it as the cost index, the

performance index, or rather the cost function.

Example: Typical use of the cost index could be the propellant used to launch a spacecraft into orbit, rather than the time of flight between orbital points, or the energy required [34] (other applications highlited in [35], [36]).

L is referred to as the path cost [37], whereas $\boldsymbol{\phi}$ is referred to as the terminal cost. Generalizing the problem, the n state variables could be subjected to various number of constraints. Let us impose then algebraic path constraints of the form

$$\boldsymbol{g}[\boldsymbol{x}(t), \boldsymbol{u}(t), t] = \mathbf{0} \tag{3.60}$$

$$\boldsymbol{g}[\boldsymbol{x}(t), \boldsymbol{u}(t), t] < \mathbf{0} \tag{3.61}$$

referred to as Equality (Equation 3.60)and Inequality (Equation 3.61) Constraints. Nonetheless, path constraints can also be categorized based on whether the correlation with the function defining the constraints refers only to the control variable or rather the state variable ([38]). Let us define then:

$$\text{Pure Control Constraints} \quad :\rightarrow \quad \boldsymbol{g}[\boldsymbol{u}(t), t] \leq \mathbf{0} \tag{3.62}$$

$$\text{Pure State Constraints} \quad :\rightarrow \quad \boldsymbol{g}[\boldsymbol{x}(t), t] \leq \mathbf{0} \tag{3.63}$$

Expression given in Equation 3.59 refers to the Bolza formulation of the problem, as it accounts for final cost into the performance index. Equivalent forms of the optimization problem have been provided by Lagrange and Mayer.

$$\text{Lagrange}: \quad J = \int_{t_0}^{t_f} L(\mathbf{x}(t), \mathbf{u}(t), t)dt \tag{3.64}$$

$$\text{Mayer}: \quad J = \phi(x(t_f), t_f) \tag{3.65}$$

Proof of their equivalence can be shown in [38].

Fuel Optimal Problem Let us consider now the situation in which we want to specify the cost function in terms of the parameter we want to optimize [39]. The statement of the problem doesn't change in its general form, obviously, but more specifically we might be asked to specify some constraints depending on the optimization required. The

performance index considered for the fuel-optimal problem reads:

$$J = \int_{t_0}^{t_f} u dt \tag{3.66}$$

Time Optimal Problem The performance index associated with the time optimal problem is then given by:

$$J = \int_{t_0}^{t_f} 1 dt \tag{3.67}$$

Furthermore, let us introduce a set of m Lagrange multipliers [40], [41], [42], allowing the n state variables to be treated as independent. The performance index introduced above is then modified, adjoining the constrained dynamics through costates variable $\boldsymbol{\lambda}$ (Lagrange multipliers).

$$\bar{J} = \phi\left[\boldsymbol{x}(t_f), t_f\right] + \int_{t_0}^{t_f} \left\{L(\boldsymbol{x}, \boldsymbol{u}, t) + \lambda^T \left\{\boldsymbol{f}(\boldsymbol{x}, \boldsymbol{u}, t) - \dot{\boldsymbol{x}}\right\}\right\} dt \tag{3.68}$$

It can be proved that the optimality condition applied to J also applies to $\bar{J}$ [43]. The introduction of the Lagrange multipliers [44], therefore, allows to reduce a variation problem with auxiliary conditions to a free variation problem without auxiliary conditions. The integrand L of the given variational problem is, in fact, modified adding the left-hand sides of the auxiliary conditions, each one multiplied by an undetermined factor λ.
For convenience, now, let us introduce the Hamiltonian function, defined as

$$\mathcal{H}\left[\boldsymbol{x}(t), \boldsymbol{u}(t), \boldsymbol{\lambda}(t), t\right] = L\left[\boldsymbol{x}(t), \boldsymbol{u}(t), t\right] + \boldsymbol{\lambda}^T(t)\left[\boldsymbol{x}(t), \boldsymbol{u}(t), t\right] \tag{3.69}$$

Integrating by parts the last term of Equation 3.68, the modified cost index can be written in the form:

$$\bar{J} = \phi\left[\boldsymbol{x}(t_f), t_f\right] - \boldsymbol{\lambda}^T(t_f)\boldsymbol{x}(t_f) + \boldsymbol{\lambda}^T(t_0)\boldsymbol{x}(t_0) + \int_{t_0}^{t_f} \left\{\mathcal{H}\left[\boldsymbol{x}(t), \boldsymbol{u}(t), t\right] + \dot{\boldsymbol{\lambda}}^T(t)\boldsymbol{x}(t)\right\} dt \tag{3.70}$$

Let us know consider the variation of the performance index due to the variations of the input control vector $\boldsymbol{u}$

$$\delta\bar{J} = \left[\left(\frac{\partial\phi}{\partial x} - \boldsymbol{\lambda}^T\right)\delta\boldsymbol{x}\right]_{t=t_f} + \left[\boldsymbol{\lambda}^T\delta x\right]_{t=t_0} + \int_{t_0}^{t_f} \left[\left(\frac{\partial \boldsymbol{H}}{\partial \boldsymbol{x}} + \dot{\boldsymbol{\lambda}}^T\right)\delta\boldsymbol{x} + \frac{\partial \boldsymbol{H}}{\partial \boldsymbol{x}}\delta\boldsymbol{u}\right] dt \tag{3.71}$$

The choice of the Lagrange Multipliers can allow us to make the coefficients of the $\delta\boldsymbol{x}$ vanish. The resulting formulation of the costate dynamics along with the control equation

define the so-called Euler Lagrange Equations

$$\begin{cases} \dot{\boldsymbol{x}} = \frac{\partial \boldsymbol{H}}{\partial \boldsymbol{\lambda}} \\ \dot{\boldsymbol{\lambda}} = -\frac{\partial \boldsymbol{H}}{\partial \boldsymbol{x}} \\ \boldsymbol{0} = \frac{\partial \boldsymbol{H}}{\boldsymbol{u}} \end{cases} \tag{3.72}$$

with boundary conditions:

$$\begin{cases} \boldsymbol{x}_0 = \boldsymbol{x}_0^* \\ t_0 = t_0^* \\ \boldsymbol{\lambda}_f = \left(\dfrac{\partial \phi}{\partial \boldsymbol{x}} \right)^T \\ \mathcal{H}_f = -\dfrac{\partial \phi_f}{\partial t_f} \end{cases} \tag{3.73}$$

Moreover, let the functions L and f be time-independent (not explicit function of t), therefore, the hamiltonian $\mathcal{H}$ will not be dependant on time explicitely, and let u(t) be an optimal program, meaning $\partial \mathcal{H} / \partial \boldsymbol{u} = 0$. We then have:

$$\dot{\mathcal{H}} = 0, \quad \text{or} \quad \mathcal{H} = \text{constant on the optimal trajectory} \tag{3.74}$$

Stationarity of the problem, and the local minimum necessary condition for J is found also by holding $\dot{\boldsymbol{x}} - \boldsymbol{f} = 0$ and requiring that the second-order expression for δJ must be non-negative:

$$\delta J = \frac{1}{2} \left[\delta \boldsymbol{x}^T \frac{\partial^2 \phi}{\partial \boldsymbol{x}^2} \delta \boldsymbol{x} \right]_{t=t_f} + \frac{1}{2} \int_{t_0}^{t_f} \left[\delta \boldsymbol{x}^T, \delta \boldsymbol{u}^T \right] \begin{bmatrix} \dfrac{\partial^2 \mathcal{H}}{\partial \boldsymbol{x}^2}, & \dfrac{\partial^2 \mathcal{H}}{\partial \boldsymbol{x} \partial \boldsymbol{u}} \\ \dfrac{\partial^2 \mathcal{H}}{\partial \boldsymbol{u} \partial \boldsymbol{x}}, & \dfrac{\partial^2 \mathcal{H}}{\partial \boldsymbol{u}^2} \end{bmatrix} \begin{bmatrix} \delta \boldsymbol{x} \\ \delta \boldsymbol{u} \end{bmatrix} dt \geq 0 \tag{3.75}$$

Pontryagin's Minimum Principle

The Pontryagin's Minimum Principle [45] outlines the condition where the control law $\boldsymbol{u}(t)$ should minimize the Hamiltonian, on the condition that $\boldsymbol{u}^*$ is part of the allowable controls in set $\boldsymbol{u}^* \in \mathbb{U} \subset \mathbb{R}^m$.

$$\boldsymbol{u}^* = argmin \left\{ \mathcal{H}(x, u, \lambda, t) \right\} \tag{3.76}$$

The control equation's validity for the Optimal Control Problem (OCP) is contingent upon the inclusion of path constraints within the Hamiltonian definition, and it is confirmed only when control constraints are inactive. However, if the Hamiltonian stationary point

regarding controls is not a member of U, then the condition fails. Pontryagin's Minimum Principle serves as a broader version of the Hamiltonian control equation and remains applicable even if the Hamiltonian formulation overlooks pure control path constraints for simplicity.

3.2.2. Non Linear Programming (NLP)

To summarize the discussion, it is important to highlight the connection between optimal control and nonlinear programming problems. The key challenge with this process is enabling human modelers (i.e., users) to easily formulate complex problems while producing an NLP that can be quickly solved by an external NLP solver [46]. The obvious step to transcript the problem is to translate the problem from a continuous-time formulation into a discrete-time one. In this way, methods such Sequential Quadratic Programming, Interior-Based or Gradient-based one aim to minimize the objective function acting on a set of variables subject to constraints.
Let us now formulate the problem in terms of NLP variables, defined as

$$\boldsymbol{y} = [\boldsymbol{x}_1, \boldsymbol{u}_1, ..., \boldsymbol{x}_M, \boldsymbol{u}_M] \tag{3.77}$$

The Optimal Control Problem above-formulated led to the minimization of the objective function $\mathcal{J}$ subjected to constraints.Substituting the discretized set of variables the new statement of the problem in terms of NLP variables can now be formulated. In particular the transcription of the objective function reads

$$J = \phi(x(t_f), t_f) + \int_{t_0}^{t_f} L(\mathbf{x}(t), \mathbf{u}(t), t)dt \tag{3.78}$$

$$\Downarrow$$

$$\bar{J} = \phi(x_M, t_M) + \sum_{i=1}^{M} L(\mathbf{x}_i, \mathbf{u}_i, t_i) \tag{3.79}$$

Constraints imposed can be transcripted in a set of equality and inequality constraints, having:

$$\min \bar{J}(\boldsymbol{y}) \quad \text{s. t.} \quad \begin{cases} \boldsymbol{h}(\boldsymbol{y}) = \mathbf{0} \\ \boldsymbol{g}(\boldsymbol{y}) \leq \mathbf{0} \end{cases} \tag{3.80}$$

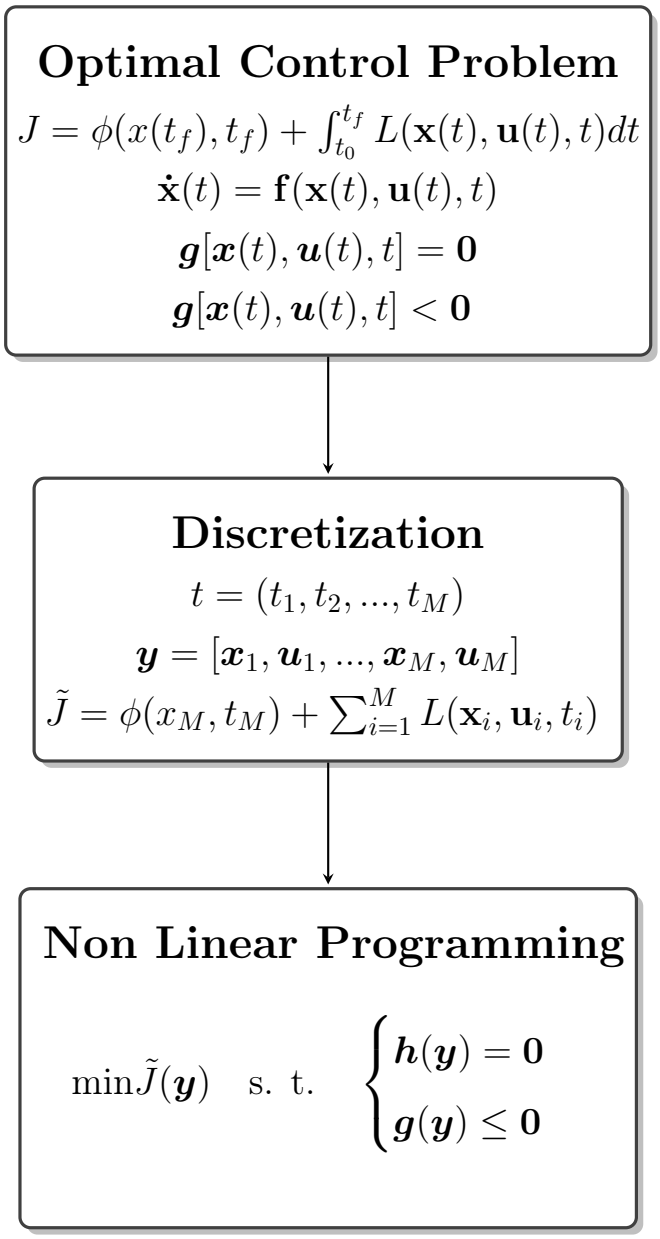

Figure 3.5: OCP to NLP transcription

3.2.3. Penalty Functions

Typically, a "one-off" nonlinear program of a certain form is expected to be feasible in normal circumstances, as infeasibility usually indicates a coding or formulation error. Nonetheless, detecting infeasibility may be crucial in specific cases, such as mixed integer nonlinear programming where it is likely to occur during branch and bound fathoming criteria. To address this, a related regularized problem can be defined, which always has feasible points. This involves formulating an alternative problem that is always well-posed and has a solution ($\boldsymbol{x}^*$) when it exists [47], [48]. By relaxing the constraints enough to

allow for feasibility, the problem can be solved while gradually reducing the amount of relaxation. Thus, the question of solution existence revolves around whether the constraints can be made feasible. This reduces to the formulation of the elastic problem [49] introducing the elastic variable $\boldsymbol{u} \in \mathbb{R}^n$ and $\boldsymbol{v} \in \mathbb{R}^m$:

$$\begin{aligned} \underset{\boldsymbol{x}\in\mathbb{R}^n;\boldsymbol{u},\boldsymbol{v}\in\mathbb{R}^m}{\text{minimize}} \quad & \boldsymbol{f}(\boldsymbol{x}) + \rho e^T \boldsymbol{u} + \rho e^T \boldsymbol{v} \\ \text{subject to} \quad & \boldsymbol{c}(\boldsymbol{x}) - \boldsymbol{u} + \boldsymbol{v} = \boldsymbol{0}, \quad \boldsymbol{x} \geq \boldsymbol{0} \quad \boldsymbol{u} \geq \boldsymbol{0}, \quad \boldsymbol{v} \geq \boldsymbol{0} \end{aligned} \tag{3.81}$$

where ρ is defined as the elastic weight, equivalent to a "penalty" on the elasticity.

$$\underset{\boldsymbol{x}\in\mathbb{R}^n}{\text{minimize}} \ \boldsymbol{f}(\boldsymbol{x}) + \rho \sum_{i=1}^{m} |c_i(\boldsymbol{x})| \quad \text{subject to } \boldsymbol{x} \geq 0 \tag{3.82}$$

If ρ is sufficiently large and $(\boldsymbol{x}^*)$ is optimal for (1.2), then it is also optimal for the elastic problem with $\boldsymbol{u} = \boldsymbol{v} = \boldsymbol{0}$, therefore the elastic problem is called an exact regularization. Two basic types of penalty functions exist:

- **Exterior Penalty functions** which penalizes infeasible solutions
- **Interior Penalty function** which penalizes feasible solutions

An optimal solution requires that a constraint is active, so that this optimal solutions lies on the boundary between feasibility and infeasibility.
Three degrees of exterior penalty functions exist:

- *barrier methods*, where no feasible solution is considered
- *Partial penalty functions*, in which a penalty is applied near the feasibility boundary
- *global penalty functions*, that are applied throughout the infeasible region

3.2.4. Penalty methods for Inequality and Equality Constraints

Section 3.2.3 highlights the penalty methods used with the assumption of no equality constraints, or either that have been converted to inequality constraints. In particular this conversion can bring unnecessary complication to the problem analyzed, causing possible violation of linear independence. Let us then formulate the constrained optimization problem $\mathcal{P}$:

$$\mathcal{P}: \quad \text{minimize } \boldsymbol{f}(\boldsymbol{x}) \quad \text{such that} \quad \begin{cases} \boldsymbol{g}(\boldsymbol{x}) \leq \boldsymbol{0} \\ \boldsymbol{h}(\boldsymbol{x}) = \boldsymbol{0} \end{cases} \quad \boldsymbol{x} \in \mathbb{R}^n \tag{3.83}$$

$g(x) \in \mathbb{R}^m$ and $h(x) \in \mathbb{R}^k$ are defined as follow:

$$\boldsymbol{g}(\boldsymbol{x}) := [g_1(\boldsymbol{x}), ..., g_m(\boldsymbol{x})]^T \quad \boldsymbol{h}(\boldsymbol{x}) := [h_1(x), ..., h_k(\boldsymbol{x})]^T \tag{3.84}$$

Penalty function definition Given the problem in the form stated above, the definition of the penalty function can now be provided.
$p(\boldsymbol{x})$ is called a penalty function [50] for P if it satisfies:

$$p(\boldsymbol{x}) = \mathbf{0} \quad \text{if} \quad \boldsymbol{g}(\boldsymbol{x}) \leq 0 \ \& \ h(x) = 0 \tag{3.85}$$

$$p(\boldsymbol{x}) > \mathbf{0} \quad \text{if} \quad \boldsymbol{g}(\boldsymbol{x}) > 0 \text{ or } \boldsymbol{h}(\boldsymbol{x}) \neq \mathbf{0} \tag{3.86}$$

The general penalty functions adopted are defined:

$$p(\boldsymbol{x}) = \sum_{i=1}^{m} [max\{0, g_i(\boldsymbol{x})\}]^q + \sum_{i=1}^{k} [h_i(\boldsymbol{x})]^q, \quad \text{where} \quad q \geq 1 \tag{3.87}$$

3.3. Low-Thrust Propulsion Systems

Low-thrust propulsion systems are characterized by their high specific impulse, typically exceeding 1000 seconds, and relatively low thrust output compared to conventional Earth launch vehicles. The key advantage of low-thrust propulsion is the ability to provide continuous thrust over a longer period of time, allowing for significant changes in a spacecraft's velocity [51].
In addition to their ability to provide continuous thrust, certain low-thrust propulsion systems offer high levels of thrusting precision. This is due to their ability to provide low-thrust over an extended period of time, combined with high levels of thrust control. This level of precision is especially useful for missions that require precise orbital adjustments. Another advantage of low-thrust propulsion is the relatively small amount of propellant that is expelled over time, which is beneficial for spacecraft with limited propellant capacity. In some cases, low-thrust propulsion can be considered as providing constant acceleration because the thrust component and the relative mass component do not change significantly over the duration of the thrusting period.

3.3.1. Electric Propulsion

Electric propulsion is the latest trend in space environment, as it proved to be over the years the most efficient propulsion system of them all, developing more and more innova-

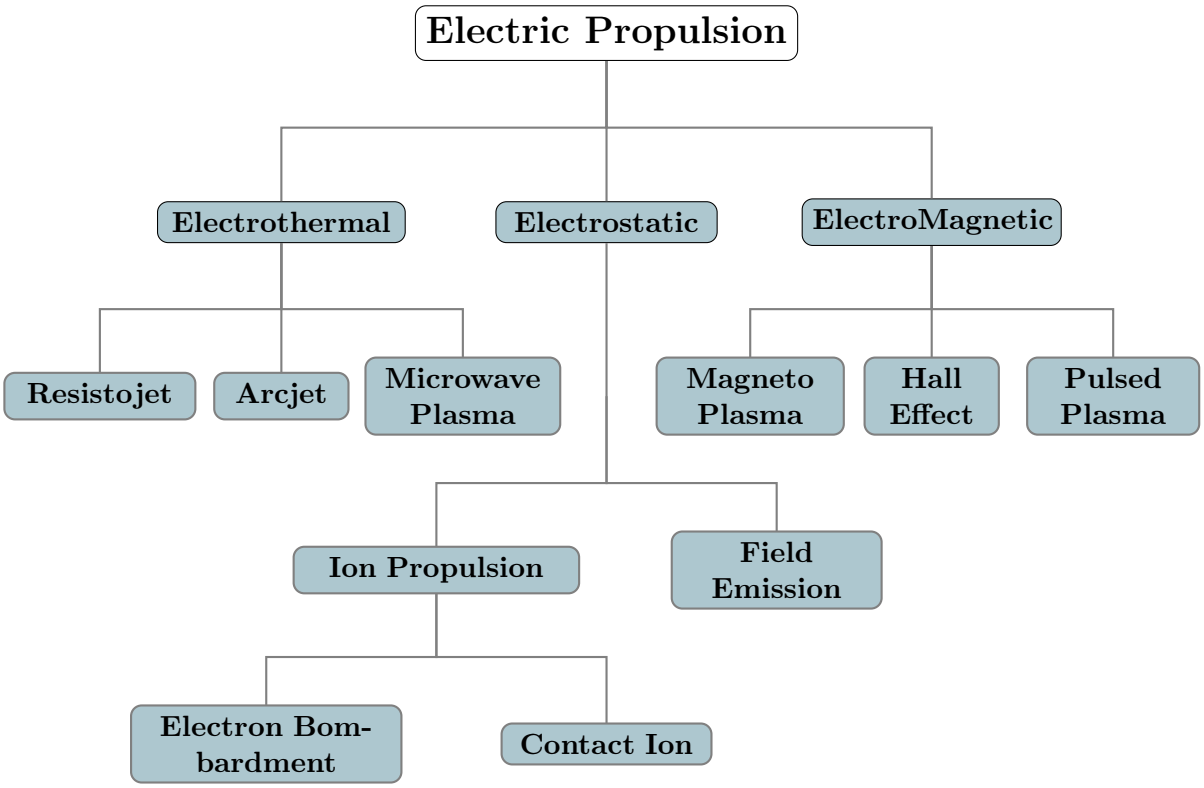

Figure 3.6: Electric Propulsion Systems Overview

tion and a wider range of applicability. Indeed, it offers several advantages, starting with safety. It is also more efficient than its chemical counterpart, as they require a much lower propellant quantity in order to have the same overall effect, as it is ejected at a much higher velocity, so obtaining a direct proportional effect in terms of propelling force. Not only in terms of consumption or safety, but rather also in terms of thrust management during the mission profile: electrical thrusters are in fact able to provide a very accurate thrust management, making it possible to perform position or attitude control along its orbit with high precision [52].

On the other hand, despite the thrust that can be applied could last for months or years, without any problem created, that is also its major limitation. Thrust level in electric propulsion are several orders of magnitudes lower with respect to chemical propulsion, so its "strength" can be considered also its major "drawback", as a thermochemical thruster can achieve the same maneuver in relatively small amounts of time. The dependence of the mission on the time, with respect to the maneuver that has to be applied, becomes then a major design "point", for which the choice of the propulsion system has to be operated with knowledge. Several electric propulsion technologies, including the Xenon ion-thruster, electron bombardment thruster, Hall effect thruster, arcjet, and resistojet, have reached technological maturity and can be utilized on spacecraft. However, mag-

netoplasmadynamic thrusters, contact ion thrusters, and pulsed induction thrusters have only been studied theoretically or in laboratory settings and are not yet advanced enough for practical use [53].

Electric Propulsion Technologies		
Technology	**Thrust Range**	**Specific Impulse Range [sec]**
Electrothermal	0.5 - 100 mN	50 - 185
Electrosprays	10 μN - 1 mN	225 - 5,000
Gridded Ion	0.1 - 20 mN	1000 - 3500
Hall-Effect	1 - 60 mN	800 - 1950
Pulsed Plasma and Vacuum Arc Thrusters	1 - 600 μN	500 - 2400
Ambipolar	0.25 - 10 mN	400 - 1400

Table 3.1: Current Electric Propulsion Technologies

3.3.2. Chemical Propulsion

On the other hand, the continuously operated propulsion subsystem using chemical propellant may not be discarded, as they have long heritage in the space environment, together with their reliability. The majority of the propulsion subsystems adopted, in fact, are mostly of this type, as the range of mission that they can be used for is very wide, from space launch systems to in-space maneuvering or attitude control. The big problem with it, though, is that the subsystem design still remains quite complex, as tanks, pipes and valves have to be designed carefully, not to forget highly inflammable propellant.
Depending on the mission profile, a variety of thrusters can be adopted.

Chemical Propulsion Technologies		
Technology	**Thrust Range**	**Specific Impulse Range [sec]**
Hydrazine Monopropellant	0.25 - 25 N	200 - 285
Alternative Mono- and Bipropellants	10 mN - 120 N	160-310
Hybrids	1 - 230 N	215 - 300
Cold / Warm Gas	10 μN - 3 N	30 - 110
Solid Motors	0.3 - 260 N	180 - 280
Propellant Management Devices	N/A	N/A

Table 3.2: Current Chemical Propulsion Technologies

4 | Software Implementation

The focus is now shifted on the actual development of the maneuver optimization tool. The key to a robust and reliable implementation is to incorporate low-thrust propulsion models along with optimization techniques.
It is for this reason, that the existing preliminary tool for design of transfer orbits is integrated now in a wider tool, which include an accurate architecture model and the physical implementation of the performed maneuver.

4.1. Spacecraft Architecture

One of the key advantages of GMAT is its ability to simulate the behavior of a spacecraft in a wide range of environments and mission scenarios. It allows users to model the motion of a spacecraft in various gravitational fields, atmospheric drag, solar radiation pressure, and other environmental factors. This enables users to predict the trajectory and behavior of a spacecraft in different mission scenarios.
Another important aspect of spacecraft architecture in GMAT is the ability to model different types of propulsion systems. The software includes models for both chemical and electric propulsion systems, as well as solar sails and other novel propulsion technologies. The advantage of the GMAT software in mission trajectory design is the simplicity of implementation of spacecraft hardware components. The details of the spacecraft model implemented represented are given in Table 4.1

Spacecraft Architecture	
Dry Mass $[kg]$	70
Drag Coefficient $[-]$	2.2
Reflectivity Coefficient $[-]$	1.8
Drag Area $[m^2]$	1.13

Table 4.1: Spacecraft architecture

In particular considering the two propulsion system used, the tanks and the thruster have

to be differentiated obviously. The properties[1] attributed to the different architecture are:

Chemical Propulsion	
Fuel Mass $[kg]$	15
Fuel Density $[kg/m^2]$	1260
Temperature $[°C]$	20
Pressure $[kPa]$	1500
Tank Volume $[m^3]$	0.75

Electric Propulsion	
Fuel Mass $[kg]$	5

The solar electric propulsion requires a further component, identified as the solar power system, considering eclipse period in which the spacecraft is in the Earth's shadow. As there are no current considerations of a realistic electric propulsion system, the only feature considered is the starting epoch of the mission, in this way the software computes the eclipse events during the maneuver.
With more accurate details the analysis can be refined considering Annual Decay Rate and margins to be applied.
When considering shadows in a solar power system model, it's important to note that there may be discontinuities in the force model when the available power for propulsion drops below a thruster's minimum usable power setting. As a spacecraft transitions from penumbra to umbra and the power available for thrusting reaches zero, the thrust acceleration can abruptly terminate, creating issues when using adaptive step integrators. In such cases, there are a few options available. For instance, fixed step integration can be used with no error control or configure the integrator to continue propagating even if a bad step (such as a small discontinuity) occurs.

4.1.1. Propagator & Force Model

The GMAT Propagator object allows us to choose among a suite of numerical integrators implementing Runge-Kutta and predictor corrector methods. An overview of the different propagator available and their integration in the GMAT Base can be found in Appendix C.
The selected one is the embedded RungeKutta89 propagator, an adaptive step, ninth order Runge-Kutta integrator with eighth order error control.

$$\frac{dr^i}{dt} = f(t, r) \tag{4.1}$$

[1]Properties attributed are assumed since no actual propulsion system has been evaluated for the analysis

The method takes an integration step, h, by separating the interval into several stages (usually of smaller size) and calculating estimates of the integration result at each stage. At each stage, the results that are being used are the ones coming from the earlier stage. The cumulative effect of the integration is an approximate total step δt, accurate to a given order in the series expansion of the differential equation, for the state variables $r_i\left(t+\delta t\right)$ given the state $r_i(t)$.
The time increment for a given stage is given as a multiple a_i of the total time step desired; thus for the $i-th$ stage the interval used for the calculation is $a_i\delta t$; the estimate of the integrated state at this stage is given by

$$k_i^{(n)} = \delta t f\left(t + a_i\delta t, r^{(n)}(t) + \sum_{j=1}^{i-1} b_{ij}k_j^{(n)}\right) \tag{4.2}$$

where b_{ij} contains a set of coefficients specific to the Runge-Kutta instance being calculated. Given the results of the stage calculations, the total integration step can be calculated using another set of coefficients, c_j and the equation

$$r^{(n)}\left(t+\delta t\right) = r^n\left(t\right) + \sum_{j=1}^{\text{stages}} c_j k_j^{(n)} \tag{4.3}$$

The error control for these propagators is implemented by comparing the results of two different orders of integration. The difference between the two steps provides an estimate of the accuracy of the step; a second set of coefficients corresponding to this second integration scheme can be used to obtain a solution

$$r'^{(n)}\left(t+\delta t\right) = r^n\left(t\right) + \sum_{j=1}^{\text{stages}} c_j^* k_j^{*(n)} \tag{4.4}$$

Stage estimates k_j and k_j^* can be selected so that they are the same; in that case, the estimate of the error in the integration $\Delta^{(n)}$ can be written

$$\Delta^{(n)} = |\sum_{j=1}^{\text{stages}} \left(c_j - c_j^*\right) k_j^{(n)}| \tag{4.5}$$

(the difference between the coefficients $c_j - c_j^*$ is the array of error estimate coefficients.) Once the estimated error has been calculated, the size of the integration step can be adapted to a size more appropriate to the desired accuracy of the integration. If the step results in a solution that is not accurate enough, the step needs to be recalculated with a smaller step size. Labeling the desired accuracy α and the obtained accuracy (calculated,

for instance, as the largest element of the array Δ), the new step used by the Runge-Kutta integrator is

$$\delta t_{new} = \sigma \delta t \left(\frac{\alpha}{\epsilon}\right)^{1/(m-1)} \tag{4.6}$$

where m is the order of truncation of the series expansion of the differential equations being solved. The factor σ is a safety factor incorporated into the calculation to avoid unnecessary iteration over attempted steps. Common practice is to set this factor to 0.9; that is the default value used in this implementation.
Similarly, if the step taken does not result in the desired accuracy, you may want to increase the step size parameter for the next integration step. The new estimate for the desired step-size is given by

$$\delta t_{new} = \sigma \delta t \left(\frac{\alpha}{\epsilon}\right)^{1/(m)} \tag{4.7}$$

The properties of the integrator have been set from the GUI. Table 4.2 reports its properties.

Runge Kutta 89 properties	
Initial Step Size	60
Accuracy	10^{-8}
Minimum Step Size	0.001
Maximum Step Size	100
Maximum Step Attempts	50

Table 4.2: Integrator Properties

GMAT provides a variety of Force Models such as point mass and spherical harmonic gravity models, atmospheric drag, solar radiation pressure, tide models, and relativistic corrections.
These contribute to have a very refined model of the orbital environment as the level of accuracy of the software is very high.

4.1.2. GMAT Optimizer

As not only the target parameters, but the maneuver itself must be optimized, the selection of an optimizer must be operated. One of the embedded solver in the GMAT software is the Yukon, a SQP-based Non-Linear Programming solver that uses an active-set line search algorithm method and a modified BFGS update to approximate the Hessian matrix.

The solver is particularly efficient handling large-scale problems with a large number of variables and nonlinear constraints.
The configuration of the solver involves the choice of different parameters including including convergence criteria, maximum iterations, and gradient computation method.
The chosen parameters are reported in the table here:

Yukon Solver Properties	
Maximum Iterations	100
Maximum Function Evals	100
Feasibility Tolerance	0.01
Optimality Tolerance	0.0001
Fucntion Tolerance	0.001
Maximum Elastic Weight	10000
Hessian Update Method	Self-Scaled BFGS

Table 4.3: GMAT Optimizer properties

Some changes will be applied with respect to the maneuver that has to be considered. This applies, in particular, when defining the properties of the control variable attached to the optimizer. These parameters, as a matter of fact, play an important role for the convergence of the optimization, as their value can determine correct numerical properties of the solver.

- **Initial Guess**: the initial guess is the starting value attributed to the optimization variable
- **MaxStep**: indicates the maximum allowed difference during one iteration to the optimal control variable
- **Perturbation**: the step size used to calculate difference derivative
- **Lower** and **Upper Bound**: The bound in which the control variable can vary

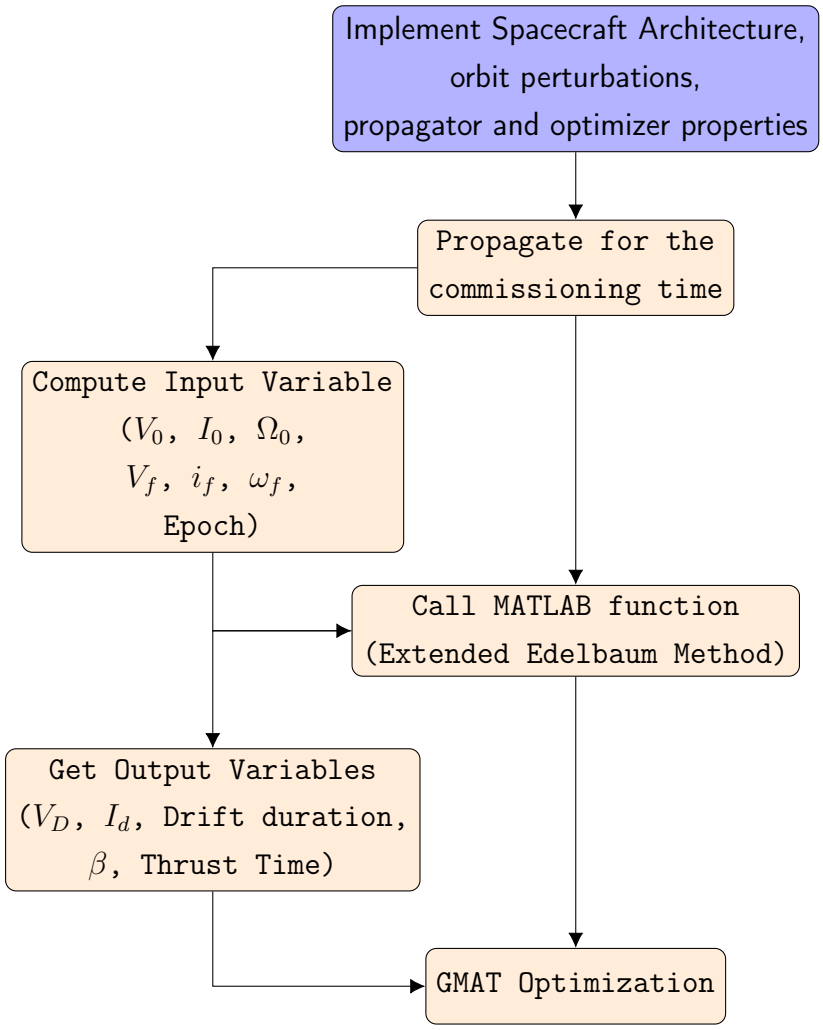

Figure 4.1: Study workflow

4.1.3. MATLAB & GMAT Interface

Once the general architecture of the spacecraft and the numerical integrators used have been created, we need to establish how to exploit the MATLAB solution of the optimal control problem.

The overall optimization that finds the initial state variable of the burn legs for the maneuver, in fact, are retrieved through the MATLAB code developed by Auckland University, developed for a RAAN matching maneuver for an active debris removal mission [54]. The two software must be therefore linked so that the propagation during the commission is operated with the accuracy of the GMAT propagator, feeding the initial orbital parameters into the MATLAB code.

The GMAT GUI (Graphical User Interface) provides the command to allow the software to communicate with the other software through some user-defined functions, providing

just the inputs and outputs necessary.

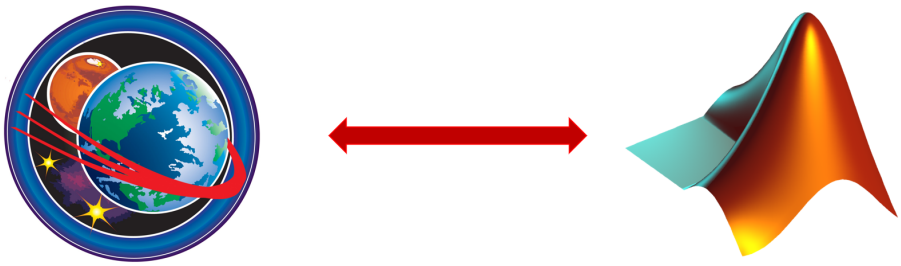

In particular, as mentioned, the analysis conducted by Edelbaum verged on inclination and velocity as independent variables. Together with the burn duration, the β angle of the thrust phase and the drift time, they are the output parameters of the MATLAB optimization in which we are interested in.
This software communication proved to be a very strong interaction, combining the best properties of both programs: the choice of using GMAT has the main software to implement the maneuver has to do, in fact, with the high accuracy of the orbit propagation due to the complexity of the perturbation models, nonetheless with the physical implementation of the spacecraft architecture; the computational ability of the Optimization Toolbox combined with the parallel toolbox in the MATLAB software, on the other hand, where exploited to provide the solution of the optimal control problem.

4.2. Split Edelbaum Strategy (SES)

The analysis conducted shows that the optimal transfer approach consists in a three-phase maneuver, that is a Thrust-Coast-Thrust strategy.
Given the starting orbital parameters (a_0, i_0, Ω_0) of the orbit and the target one we want to achieve (a_f, i_f, Ω_f) to put the satellite in its nominal orbit, we derive from the OCP the parameters of the drift orbit necessary for the minimum-fuel problem or the minimum-time problem.
As the parameter of the orbit will be modified the RAAN change will be modified as well. In this way the drift time can be optimized to achieve a RAAN matching. The RAAN, in fact, is not modified through some direct maneuver operated with the thrusters, but only varies with the Natural J_2 Drift.
Therefore, during the drift period, no thrusting procedure is considered. With a further analysis, considering drag acceleration, some in-plane maneuver may be considered in

order to counteract its effect.

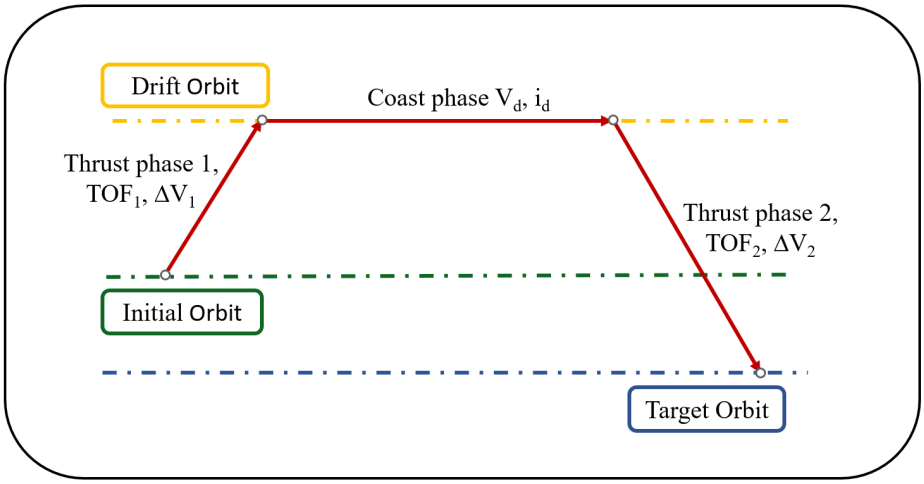

Figure 4.2: Thrust-Coast-Thrust Sequence

4.3. Formulation of the Transfer Problem

Once the general architecture and the Interface is set up, the maneuver is implemented. The solution of the optimal control problem through the MATLAB engine provided the variable we need to set up the necessary parameters for the maneuver.
As the guideline from Edelbaum establishes, the maneuver consists in a multi revolution transfer with a thruster yaw angle switch at the antinodes of the orbit. The overall maneuver is then inserted in a GMAT Optimization process which takes different optimization variable from the optimal control problem.
The choice of the low-thrust propulsion system does not allow to consider the maneuver as a quasi-impulsive maneuver, as the level of thrust obliges us to have a continuous thrust during the coast phases.
The GMAT command that enables the continuous burn for a finite period of time is the 'BeginFiniteBurn'. The amount of time of the burn is set as an optimization variable so that the amount of the thrust period is chosen as optimal. Along with the burning time, the thruster direction during the burn phase is also optimized.
As the switch of the thruster direction is performed at the node of the orbit, the thrust period will form two arcs around these points. Therefore, to optimize the burning time of the maneuver we exploit the GMAT backpropagation integrator property.

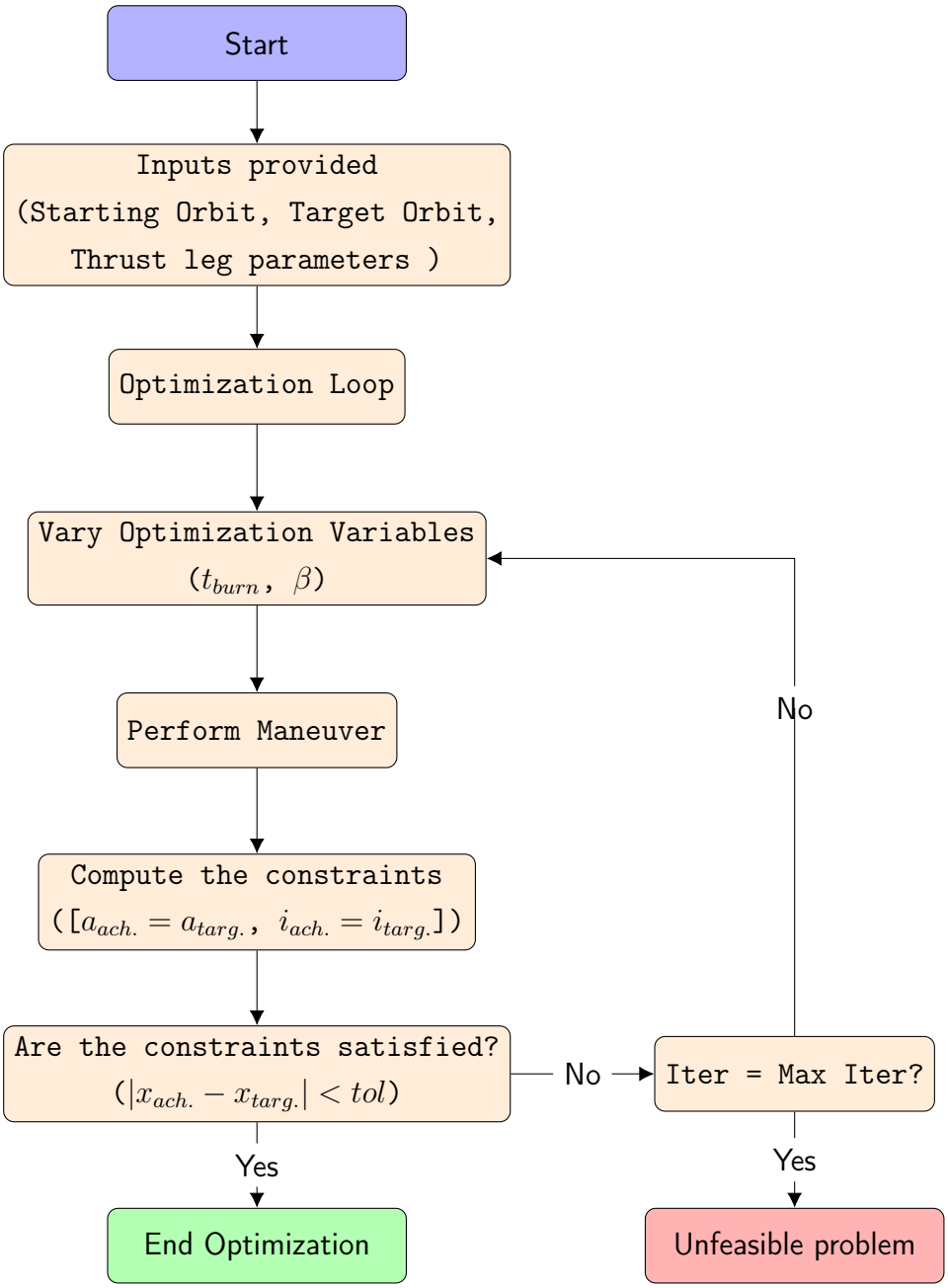

Figure 4.3: GMAT Optimization

Once the spacecraft is placed at one of the nodes, we perform the backpropagation: as the burning time is an optimization variable, we simply propagate backwards for an amount of time corresponding to the half of this value, such that the nodes of the orbit will be the points around which the thruster perform the burn.
Once the target parameters are reached the drift period begins. Here the spacecraft is naturally propagating under the effect of the perturbation for the amount of time coming from the MATLAB Optimization. Several constraints on the maximum drift

height and inclination have to be put, in order to be compliant with the permission or the technological limit of the spacecraft. This period is mostly exploited for the higher RAAN change due to the its relation with the semi major axis. So, the longer the time, the higher the variation will be.
Once the LTAN variation reaches the desired value the nominal orbit has to be reached again, so the maneuver that will put the spacecraft in its operational orbit will take place. The actual scheme of the maneuver doesn't change, so that both SMA and Inclination will be changed at the same time.
This algorithm works in the general way, but the choice of the propulsion system plays a major role in the maneuver we have to carry out.

4.3.1. Electric Propulsion System

Considering a low-thrust, 2 mN, electric propulsion system, the maneuver implemented works accordingly to the algorithm reported above. In this way, we can vary the inclination and the semi major axis at the same time, imposing the thruster yaw angle as an optimization variable. The switch of the yaw angle is performed at the antinodes, according to the Edelbaum guideline. In such way, the maneuver is performed in a unique way (maneuver algorithm reported in 4.1).

Remark: Classic guideline imposes a piecewise constant yaw angle, variable from one revolution to another. The optimization implemented however, even though it allows the optimization of the variable per revolution, considers the change in the yaw angle value in a rather poorly discretized sense, due to the increase in the problem size as we increase the number of optimization variables. In this way, the "absolute" yaw steering can only be performed few times. This computational limitation however, does not private us from finding a suitable sub-optimal solution to our problem. In this case the absolute yaw change is performed at half of the burn phase, therefore considering two β variations.

4.3.2. Chemical Propulsion System

The chemical thruster yields a different approach to the maneuver. As it stands, a 1 N thruster is a powerful type of propulsion for the purpose of the mission, so it has to be treated differently.
Numerical problems have been encountered when the variation of the semi-major axis and inclination are performed together, so the procedure taken is different.
The maneuver is divided in such a way that the thruster will perform an in-plane burn phase where only the raise in the semi major axis is made. Subsequently, a pure out-of-

Algorithm 4.1 Maneuver Implementation - Electric Propulsion

Vary T_{Burn}, β
for $i \leftarrow 1, N_{Rev}$ **do**
  Propagate to Node $(Z = 0)$
  if $AOP + TA = 360$ **then**
    Switch Thruster Direction $(+\beta)$
  else if $AOP + TA = 180$ **then**
    Switch Thruster Direction $(-\beta)$
  end if
  BackPropagation $t = T_{burn}/2$
  procedure BeginFiniteBurn
    Propagate T_{burn}
  end procedure
  Propagate to Node $(Z = 0)$
  if $AOP + TA = 360$ **then**
    Switch Thruster Direction $(+\beta)$
  else if $AOP + TA = 180$ **then**
    Switch Thruster Direction $(-\beta)$
  end if
  BackPropagation $t = T_{burn}/2$
  procedure BeginFiniteBurn
    Propagate T_{burn}
  end procedure
end for=0

plane maneuver will take place where the inclination is changed. In this way the only parameter influencing the maneuver will be the burn duration of the thrusting time and the number of revolutions for which we perform this operation. The modified algorithm used is reported in 4.2.

This type of solution presents an issue: as the propulsion system yields a 1 N thrust, the semi major axis change in the thrust phases lasts for a very short amount of time. As it stands, the eccentricity of the orbit will be certainly modified. Some corrections therefore have to be applied to the maneuver in order to reach the target value of the parameters.

The second leg of the maneuver, where the spacecraft transfers from the Drift Orbit to the target orbit where the nominal operations will be performed, should, in principle, follow the same flow in the algorithm stated above. However, the optimization shows convergence problem when both the optimization variables are varied in the same loop. Due to this problematic the two loops consisting in the in-plane and out-of-plane maneuvers will be separated, so that they will be individually optimized (4.3, 4.4).

Algorithm 4.2 Maneuver Implementation - Chemical Propulsion ($1^{st}Leg$)

Vary $T_{Burn\ SMA}$, $T_{Burn\ Inc}$
Switch Thruster Direction (In-Plane Maneuver)
for $i \leftarrow 1, N_{Rev}$ **do**
    Propagate to Periapsis
    procedure BeginFiniteBurn
        Propagate for $T_{burn\ SMA}$
    end procedure
end for
Propagate to Node
Switch Thruster Direction (Out-of-Plane Maneuver)
for $i \leftarrow 1, N_{Rev}$ **do**
    Propagate to Periapsis
    procedure BeginFiniteBurn
        Propagate for $T_{burn\ Inc}$
    end procedure
end for=0

Algorithm 4.3 Maneuver Implementation - Chemical Propulsion (2^{nd} Leg), SMA

Vary $T_{Burn\ SMA}$
Switch Thruster Direction (In-Plane Maneuver)
for $i \leftarrow 1, N_{Rev}$ **do**
    Propagate to Periapsis
    procedure BeginFiniteBurn
        Propagate for $T_{burn\ SMA}$
    end procedure
end for=0

4.4. Station Keeping

As the maneuver serves to insert the spacecraft in its nominal orbit, so that the payload can perform its operation at the best possible condition, it must be kept as close as possible in this orbit. But, as stated repeatedly, due to the effect of perturbations (mainly aerodynamic resistance as it lowers the perigee altitude, lowering therefore the altitude and altering the eccentricity), the orbit is expected to change during the operation lifetime. Some station keeping maneuvers will be definitely required (Algorithm 4.5). In order to account for this, simulating the whole mission orbit could lead to different considerations in terms of target parameters of the orbit. If, in fact, the change in the parameters (mainly RAAN), during the operations is seen to be over the performance limits of the payload, the preliminary target parameters may be altered slightly in order to compensate for this variations and guarantee a "safe" orbit maintenance.

Algorithm 4.4 Maneuver Implementation - Chemical Propulsion (2^{nd} Leg), Inc

Vary $T_{Burn\ Inc}$
Switch Thruster Direction (Out-of-Plane Maneuver)
for $i \leftarrow 1, N_{Rev}$ **do**
  Propagate to Node
  procedure BeginFiniteBurn
    Propagate for $T_{burn\ Inc}$
  end procedure
end for=0

Algorithm 4.5 Station Keeping

while Elapsed Years $<$ 5 **do**
  Propagate One Step
  if Altitude $<$ Threshold **then**
    Propagate to Periapsis
    procedure Optimize(loop)
      Vary $T_{burn\ (SMA)}$, $T_{burn\ (ecc)}$
      BackPropagation $t = -T_{burn\ raise\ SMA}/2$
      procedure BeginFiniteBurn
        Propagate for $T_{burn\ raise\ SMA}$
      end procedure
      Propagate to Apoapsis
      Switch Thruster Direction
      BackPropagation $t = -T_{burn\ raise\ SMA}/2$
      procedure BeginFiniteBurn
        Propagate for $T_{burn\ raise\ ecc}$
      end procedure
      Propagate to Periapsis
      Switch Thruster Direction
      BackPropagation $t = -T_{burn\ raise\ SMA}/2$
      procedure BeginFiniteBurn
        Propagate for $T_{burn\ raise\ ecc}$
      end procedure
    end procedure
  end if
end while=0

5 | Results and Analysis

The most relevant results obtained by both propulsion systems are here highlighted, in terms of the parameters coming out of the MATLAB optimization and the actual maneuver performed in GMAT. Differences between different final target orbit will be pointed out as intended to different final LTAN achieved and different altitude and inclination.
The amount of LTAN correction investigated [1] corresponding to the actual RAAN achieved is reported in Table 5.1

LTAN Correction	Final RAAN Achieved
2	216.34
2.5	208.84
3	201.34
3.5	193.84
4	186.34
4.5	178.84

Table 5.1: Final RAAN as function of the LTAN correction applied

5.1. Edelbaum Analytical Analysis

An auxiliary analysis has been conducted, performing the maneuver just considering the Extended Edelbaum method, just exploiting the analytical solution of the transfer, along with the integrated one, assuming constant thrust acceleration during the transfer.
Both are represented in Figure5.1 and 5.2. The results of this auxiliary analysis yield different values from the one performed in this work, mainly because of the many assumptions made for the Edelbaum transfer, and that result in different value of the burning time necessary to get to the target orbit or either the constant value of the Right Ascension (RAAN), which does not take into account the major effects of the natural drift caused by the gravity gradient. The approximations introduced therefore do not allow to consider this a high accurate solution.

[1] The analysis can be obviously generalized on any amount of correction desirable, but just to highlight how the variable change according to the target imposed, discrete values reported have been investigated

An interesting consideration can be made about the yaw angle, which proves to be consistent with our analysis. Integrated solution provided in Figure 5.2a also shows the actual change applied for every revolution, where the flip of the yaw angle is applied.
Moreover, the change in the yaw angle during the thrust (Figure 5.1a) is linear throughout the whole maneuver, however, the absolute values of the starting and final time differ of just 1°, and that's why can it be considered constant.

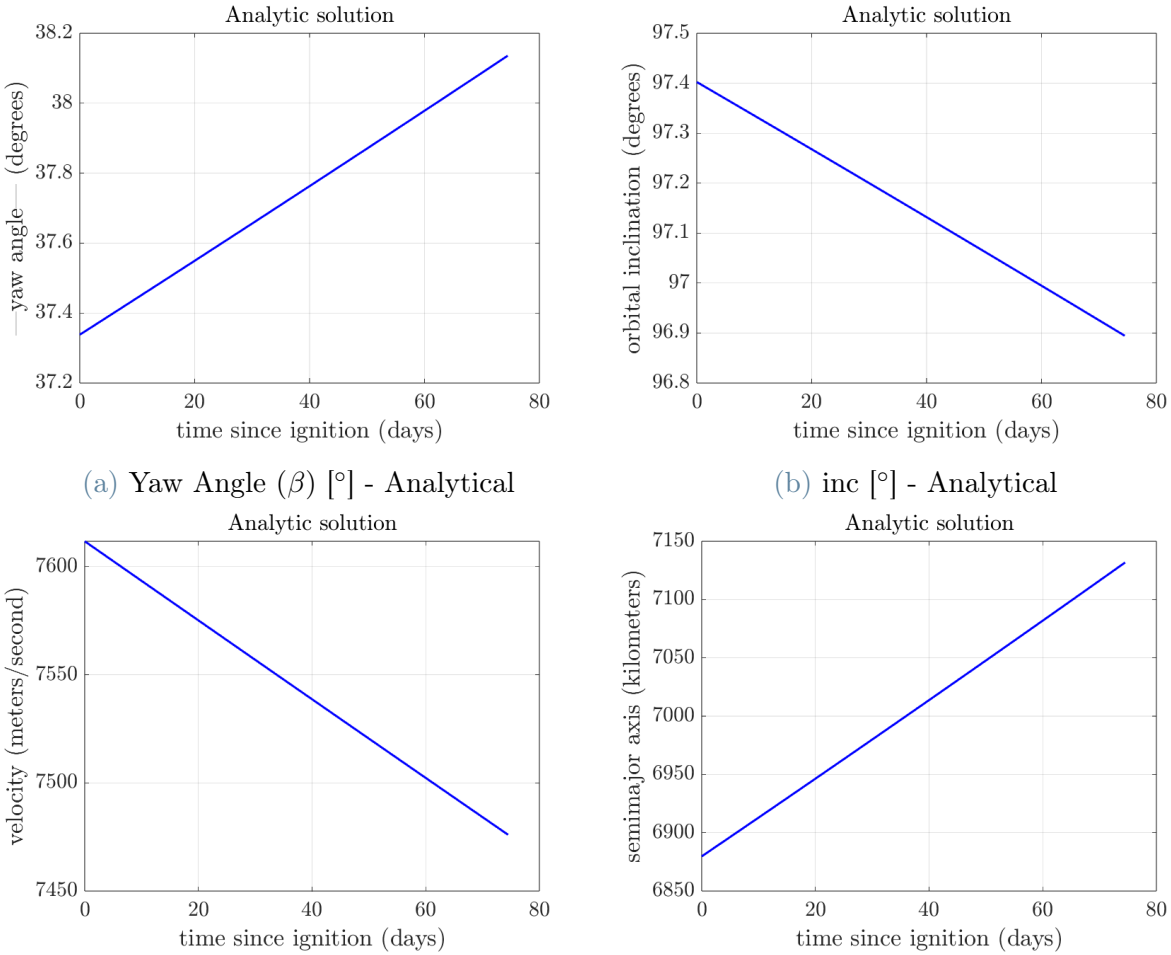

(a) Yaw Angle (β) [°] - Analytical

(b) inc [°] - Analytical

(c) Velocity [m/s] - Analytical

(d) SMA [km] - Analytical

Figure 5.1: Analytical Solution of the Edelbaum Transfer

The actual rather simple inclination change can be noted, not influenced by short-period or secular variation effects due to J_2. Semi-major axis change is also rather straightforward as the drag is not taken into account.

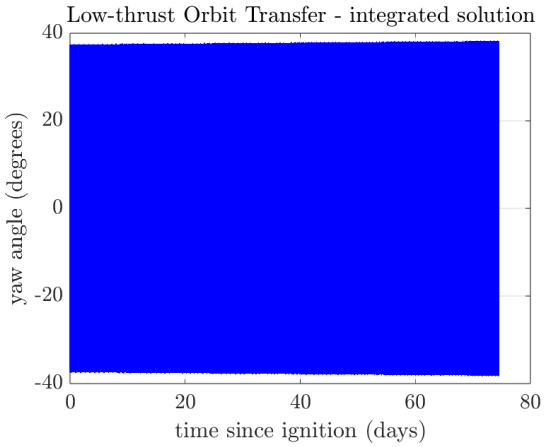

(a) Yaw Angle (β) [°] - Integrated

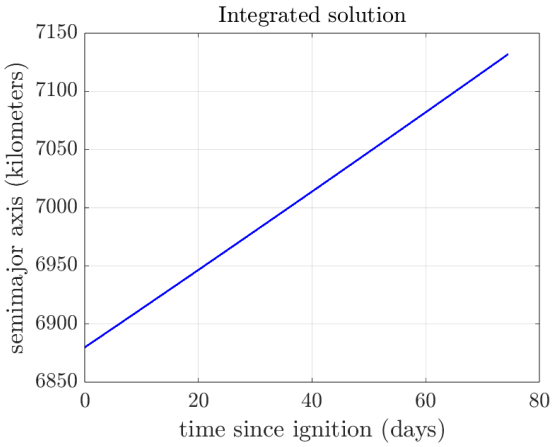

(b) SMA [km] - Integrated

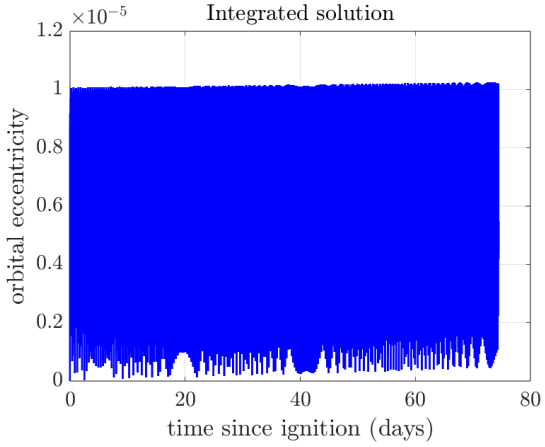

(c) Ecc [-] - Integrated

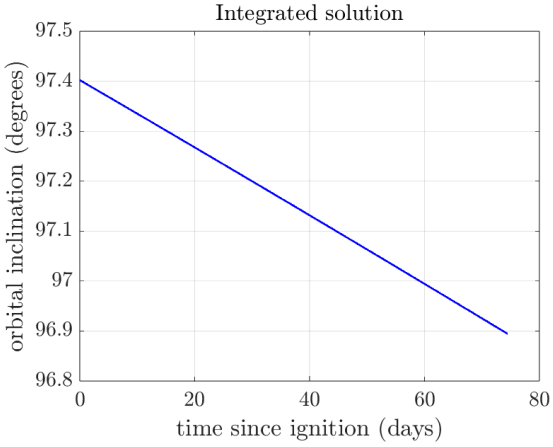

(d) inc [°] - Integrated

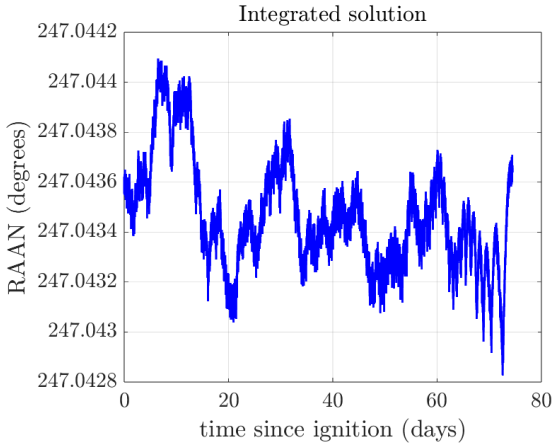

(e) RAAN (Ω) [°] - Integrated

Figure 5.2: Integrated Solution of the Edelbaum Transfer

5.2. MATLAB Optimization

Let us now move the discussion to the actual MATLAB optimization, exploiting the RAAN matching. In particular, a detailed analysis of the constraint imposed on the optimization variables and other further parameters will be carried out, considering several correction on the LTAN.
Fixing the starting parameters and giving as input the optimal problem scenario the fitness function changes accordingly. As above-stated, some constraints on the optimization variable have been fixed to perform the maneuver. No detailed information for orbit transfer permission have been provided yet, but some preliminary analysis indicate a maximum altitude reachable of approximately 1000 km, due to thermal problematic arising at higher altitudes. However, as the altitude of the drift orbit implies different values of the RAAN drift ($\dot{\Omega}$), a minimum altitude has been imposed.
Further analysis concerning orbit availability shall be performed, according to possible rules or even to possible maneuver performed for collision avoidance. No specific inclination constraint are needed, as the preliminary orbit analysis did not highlight specific needs. However, some optimizations highlighted strange behaviours when raising the inclination to get to the drift orbit, yielding a very high ΔV.
To overcome this issue the inclination has been constrained in such a way that the drift value shall be lower than the target one.

Drift Constraints	
Drift Inclination [°]	≤ 97.37
Drift SMA [km]	$\geq$ Start SMA + 100

Table 5.2: Constraints on the optimization variable

Given this linear inequality constraints provided to the optimization, the simulation is performed. The actual optimization variable couple is not defined as (a, i) but rather the velocity is used as the first variable. The formulation is however equivalent due to the relation between the two.

$$v = \sqrt{\frac{\mu}{a}} \tag{5.1}$$

Differentiating now the analysis for the specific propulsion systems, results dependant on the LTAN correction applied can be provided.

5.2.1. Electric Propulsion

In particular, considering the main propulsion system examined the following drift variables (Table 5.3) come from the MATLAB optimization

LTAN Correction	Drift Semi-Major Axis [km]	Drift Inclination [°]
2	6979.597	97.258
2.5	6970.075	97.061
3	6998.815	97.012
3.5	-	-
4	-	-
4.5	7131.645	96.895

Table 5.3: Optimization Variables vs LTAN Correction - Electric Propulsion

Unfortunately, applied correction of 3.5 and 4 hours, lead to an unfeasible problem, which therefore cannot be used as a benchmark to see the evolution of the parameters with the different maneuvers. Graphical representation of the maneuver is reported in Figure 5.3. Implementation in the GMAT software, however, is considered more accurate, due to the very high model representation of the disturbances.

5.2.2. Chemical Propulsion

Results dependant on the LTAN correction applied for the chemical propulsion are then below reported (Table 5.4)

LTAN Correction	Drift Semi-Major Axis [km]	Drift Inclination [°]
2	6990.412	97.331
2.5	6990.514	97.216
3	6990.412	97.095
3.5	7026.103	97.111
4	7051.918	97.085
4.5	7090.412	97.085

Table 5.4: Optimization Variables vs LTAN Correction - Chemical Propulsion

Drift Variables change is quite different varying the amount of correction applied. Con-

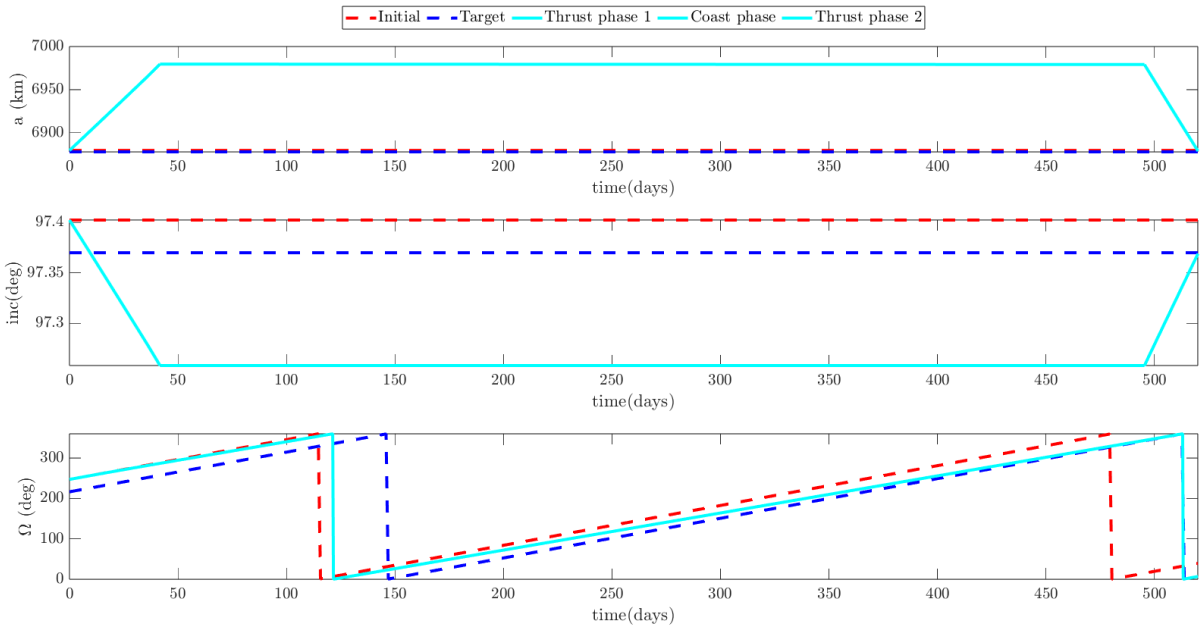

(a) 2 Hours Correction Maneuver

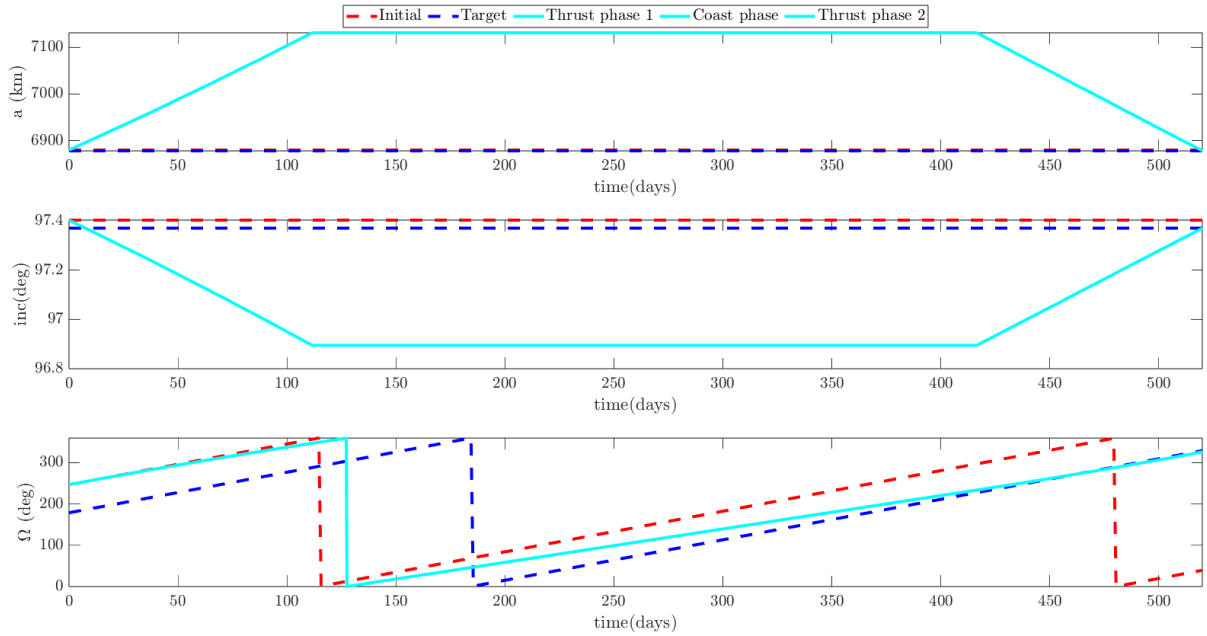

(b) 4.5 Hours Correction Maneuver

Figure 5.3: MATLAB Optimized Maneuvers - Electric Propulsion

sistently with the drift variation, higher values of the SMA and lower inclination value are observed (Figure 5.4). Both systems exploit this combination, even though the way it is exploited is quite different. We remark, in fact, that the natural RAAN drift changes during the thrust phase maneuver for the Electric Propulsion, which allows to a optimized time, meaning that the drift time in percentage is much smaller with respect to higher thrust values.
Considering, in fact, higher thrust values thrust phase, maneuver time gets radically low, allowing to exploit the maximum Drift for the higher time possible. Due to this considerations, the maneuver is "optimized", yielding a higher drift time and a lower change in the orbital parameters with the same net effect on the final result.

5.2.3. Optimization considerations

The behaviour presented by optimization parameter during the simulation is reported in Figure 5.5

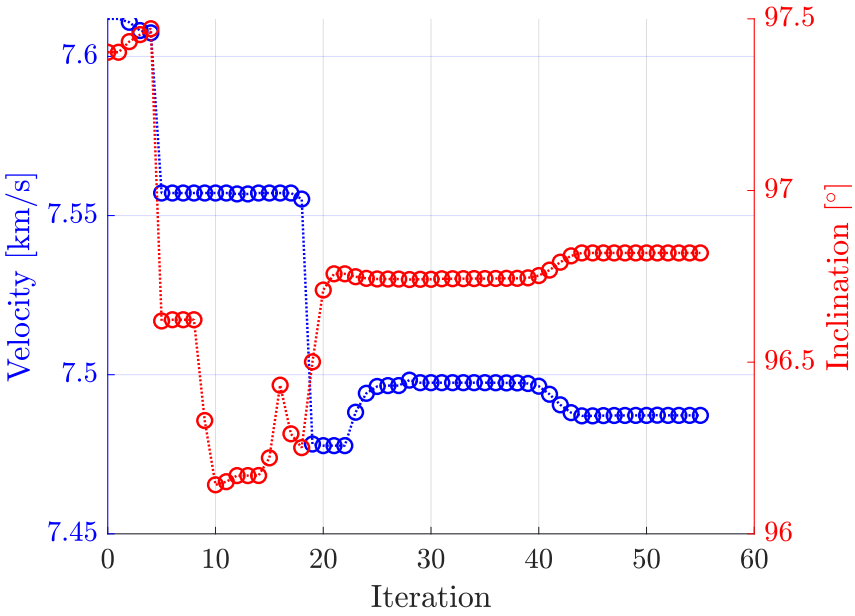

Figure 5.5: Converged variable evolution - 2 hours correction

Variation in the last iterations is very little, considering optimality and feasibility tolerances given to the solver.

Remark: Due to an extremely various number of factors (e.g: minor perturbations not considered, inaccurate modeling of perturbations, sensors and actuators accuracy) the target required is not achieved at the level of accuracy desired. Further evaluation and

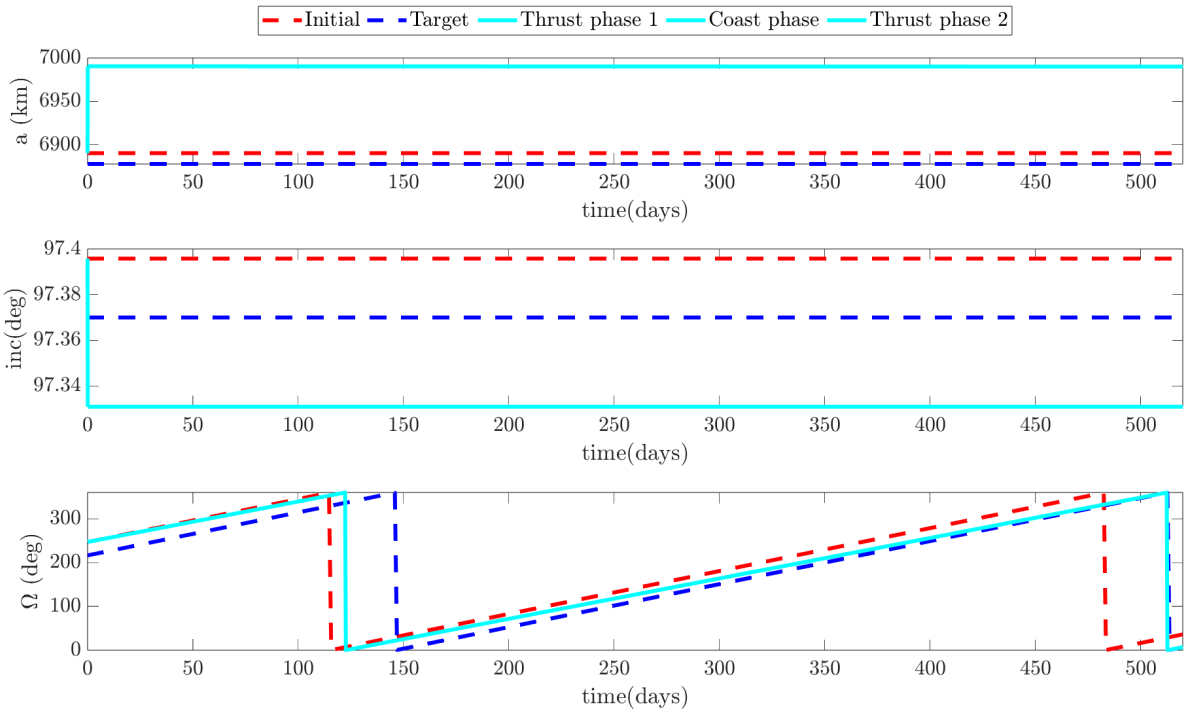

(a) 2 Hours Correction Maneuver

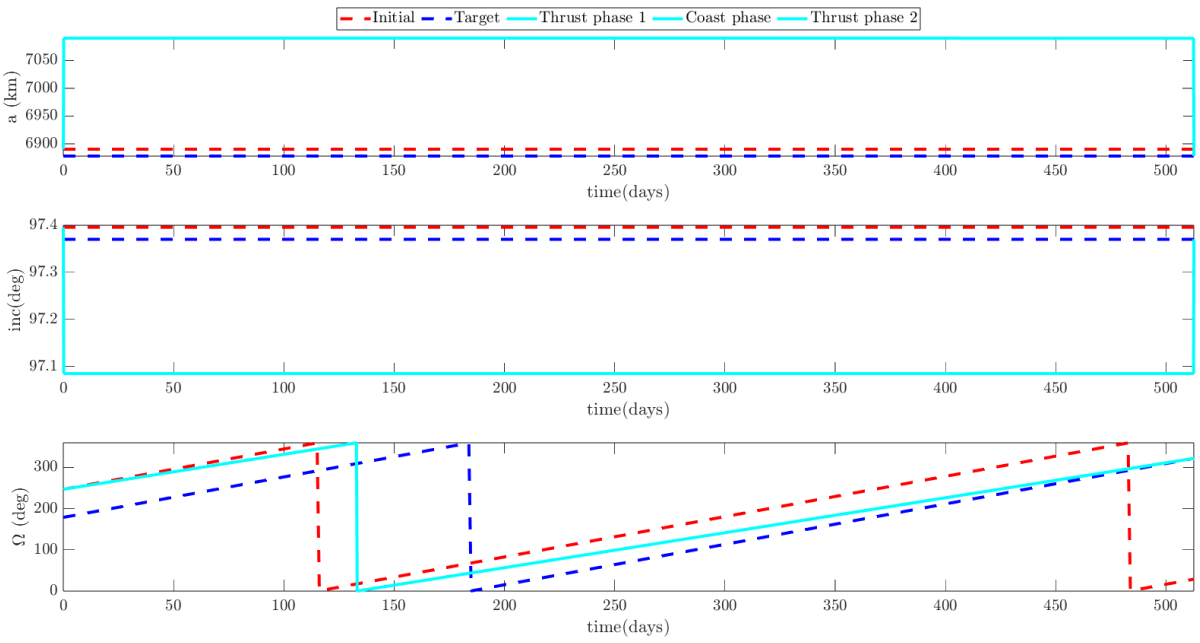

(b) 4.5 Hours Correction Maneuver

Figure 5.4: MATLAB Optimized Maneuvers - Chemical Propulsion

considerations about tolerances due to this factors have to be taken into account as the computational effort can be reduced significantly, despite having to perform the same maneuver in terms of achievable performances.

5.3. Maneuver

Once the actual parameter of the drift orbit are retrieved the GMAT simulation can be performed. Not only drift variables, but also the parameters characteristic of the thrust legs have been considered, mainly the burning time and the beta angle. These ones have been set as optimization variables for the GMAT optimization with the initial guesses set by the MATLAB output. The variation of the orbital parameters during the maneuver is reported.
Of course, varying the amount of correction imposed, the drift parameters vary accordingly, as the RAAN drift varies with the SMA and Inclination value.
As these values differs from one maneuver to the other, the amount of time that the thrusters will be turned on differs as well, and that translates into different fuel necessary to perform the maneuver.
Differentiating in the same way as it's been made for the MATLAB optimization results of the maneuver carried out for the two different propulsion systems are presented.

5.3.1. Electric Propulsion

Considering the electric propulsion[2], Table 5.5 reports the overall burning time required along with the fuel mass required.

LTAN Correction	Total Burning Time (Days)	Fuel mass consumed
2	66.612	0.663
4.5	215.229	2.221

Table 5.5: Burning time, Fuel mass vs LTAN - Electric propulsion

The time of flight sensibly change from the lowest to the highest correction imposed, according to the drift parameters change. The higher the RAAN to correct, the higher will

[2]Due to high computational effort, the analysis performed with the electric propulsion is limited only to the lowest and the highest LTAN interval considered. Nonetheless, this does not necessary imply a limitation of the tool, as the amount of correction imposed is chosen with regard to technology and operational constraints. It's not the case for the chemical propulsion, however, where the analysis can be extended for a chosen set, to see the maneuver trend

be the change in the drift variables, and, as the propulsion system can yield a maximum thrust of only 2 mN the time of flight increases significantly.

LTAN Correction	β 1st Leg	β 2nd Leg
2	28.644	157.082
4.5	37.338	143.872

Table 5.6: Yaw angles vs LTAN - Electric propulsion

Fuel mass consumption, however, despite the high thrust time, is well below the starting amount imposed.

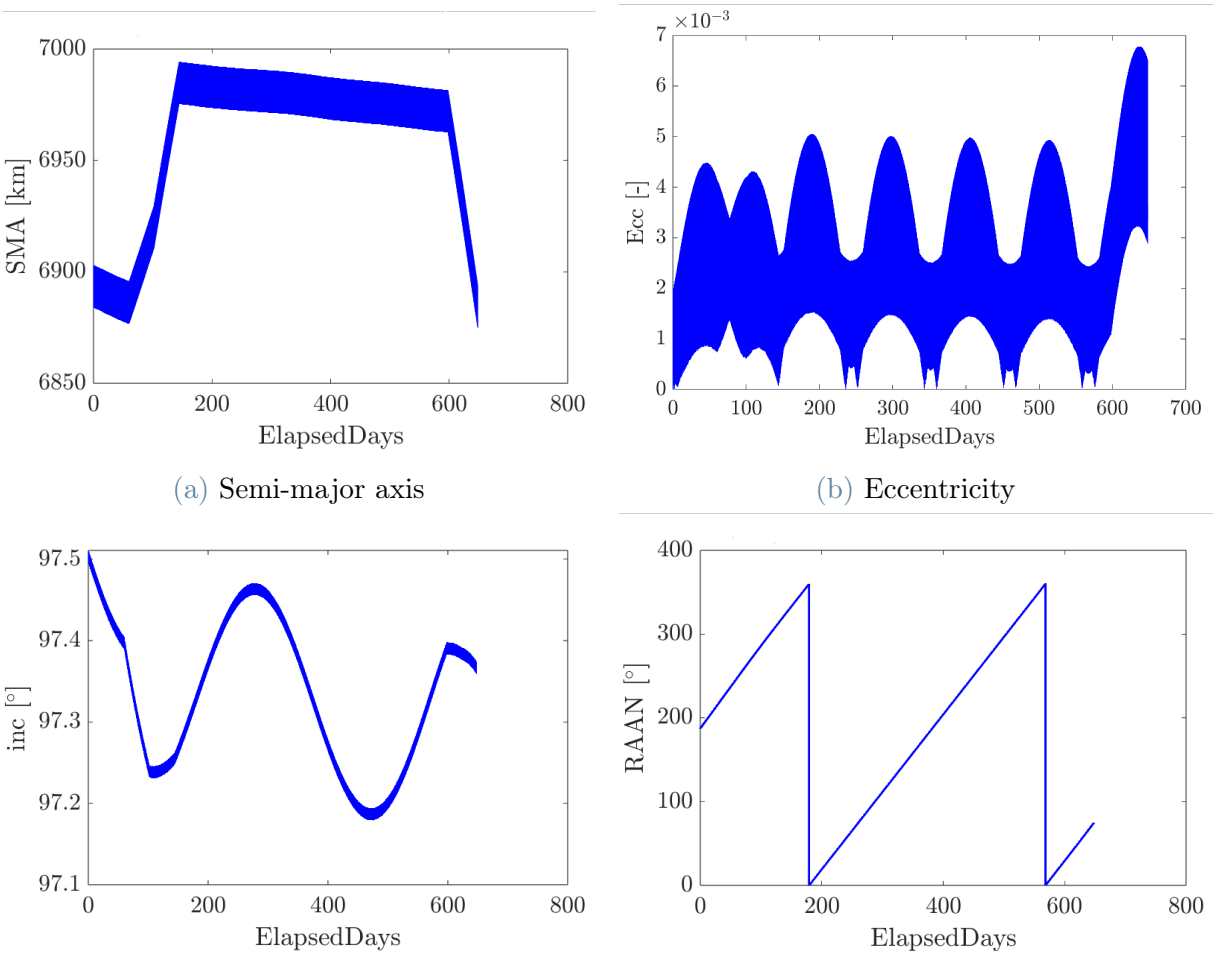

(a) Semi-major axis

(b) Eccentricity

(c) Inclination

(d) RAAN

Figure 5.6: Orbital parametrs evolution during transfer for a 2 hours LTAN correction - Electric Propulsion

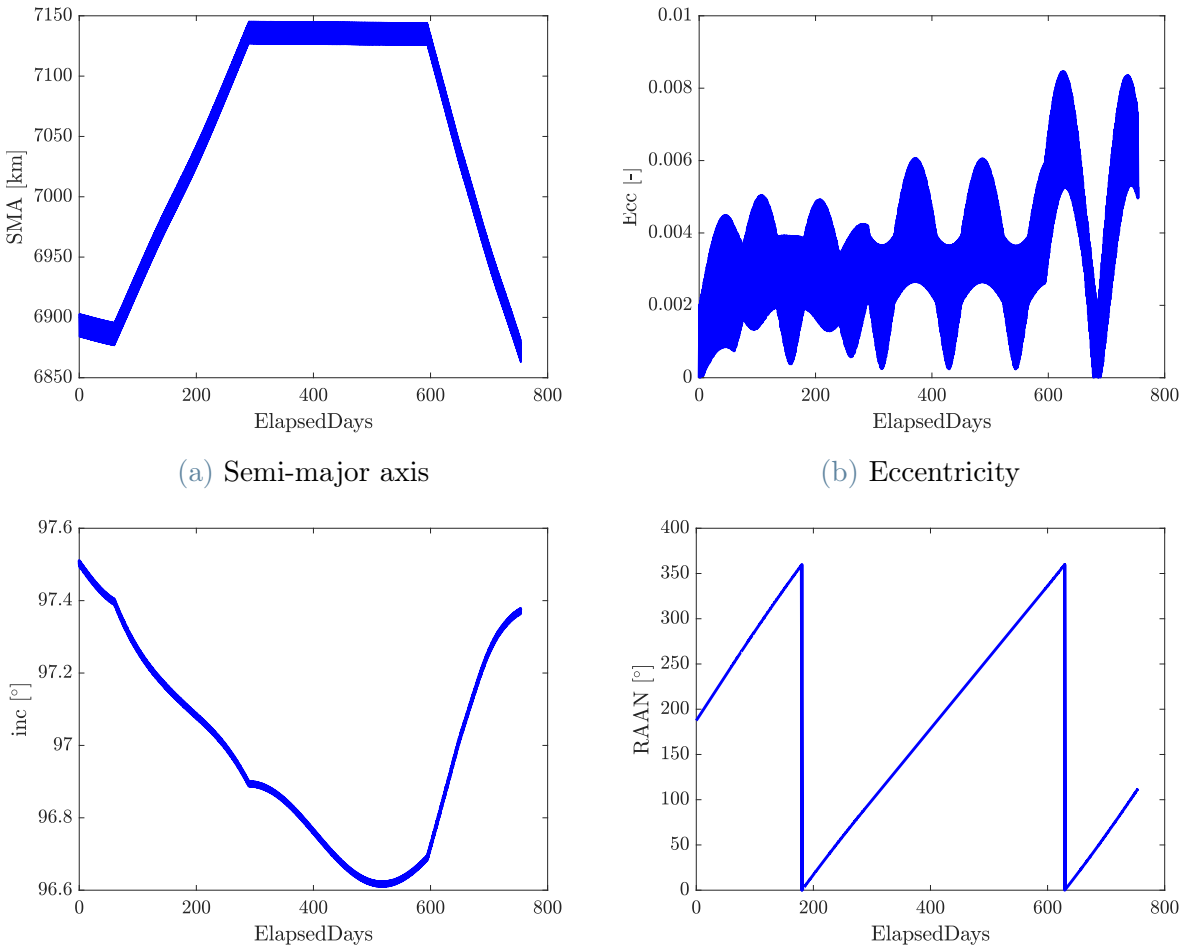

(a) Semi-major axis

(b) Eccentricity

(c) Inclination

(d) RAAN

Figure 5.7: Orbital parametrs evolution during transfer for a 4.5 hours LTAN correction - Electric Propulsion

5.3.2. Chemical Propulsion

Optimal analysis performed, provided us with the values of Yaw steering angle for both thrust legs also in the chemical propulsion. However, the maneuver is performed in a way that doesn't account for a simultaneous change in both the semi-major axis and inclination. For this reasons, the main concern is on the actual drift orbit, as we highlight the change in the parameters along with the fuel mass used for the transfer.

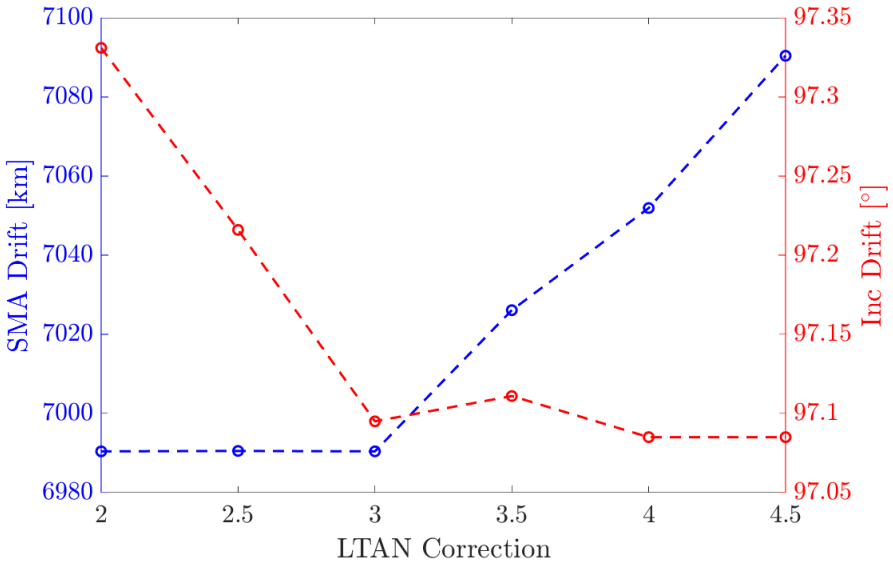

(a) Drift Parameters vs LTAN

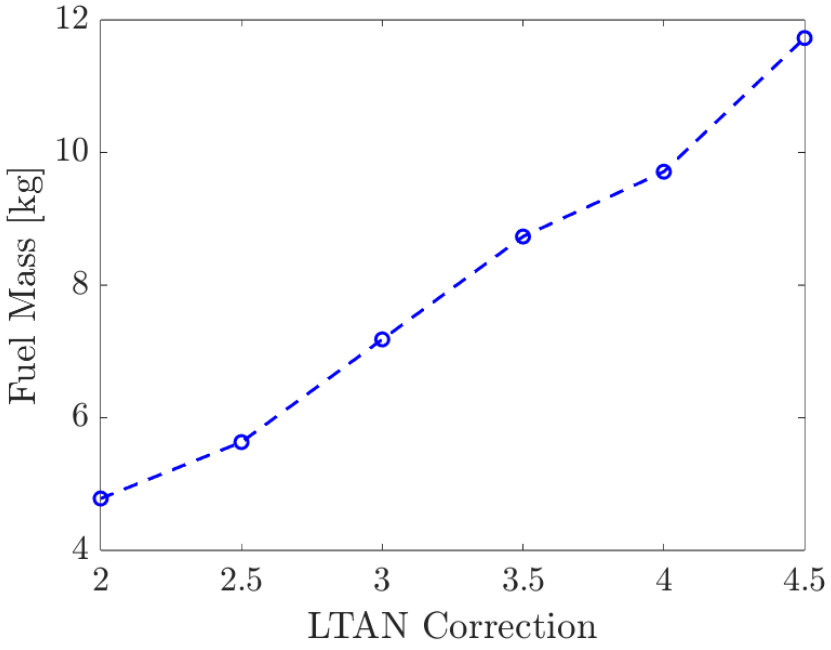

(b) Fuel Mass vs LTAN

Figure 5.8: Variation of the Optimal drift parameters and Fuel Mass consumed with the LTAN correction - Chemical Propulsion

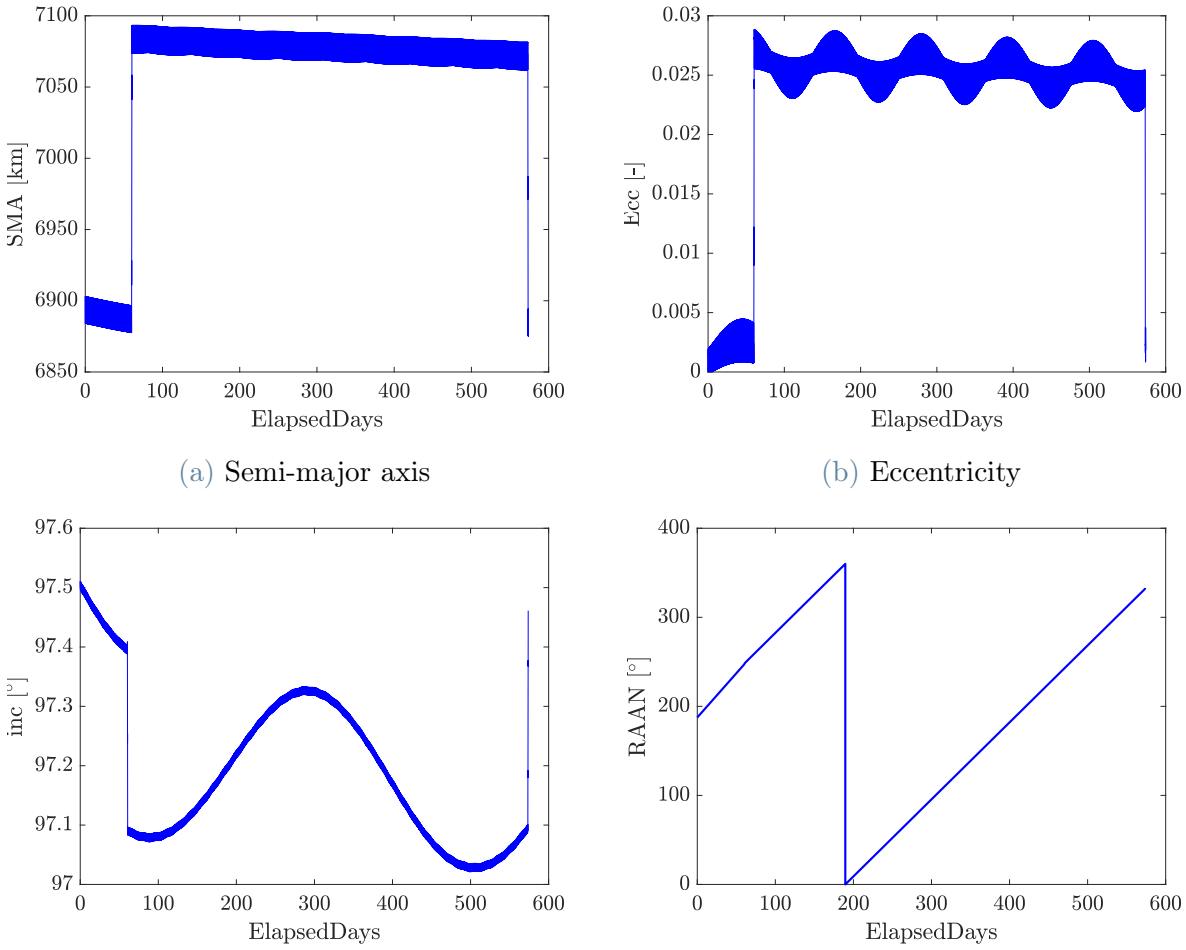

(a) Semi-major axis

(b) Eccentricity

(c) Inclination

(d) RAAN

Figure 5.9: Orbital parametrs evolution during transfer for a 4.5 hours LTAN correction - Chemical Propulsion

Noticeable changes can be seen concerning the thrust phases. Particularly as the thrust level is very different, the necessary time for the maneuver differs as well, in the order of months for the electric propulsion, whereas in days for the chemical propulsion.
In particular, the eccentricity change is quite visible, as the maneuver considered for the 1 N thrust option is performed around the periapsis rather than performing a Yaw Switch steering every half orbit. This results, therefore, in a "highly" eccentric drift orbit. However, the opposite maneuver is performed to lower the SMA in the 2nd leg, so no apparent correction has to be made.

6 | Conclusions and Future Work

6.1. Conclusions

The work carried out proved the reliability of the tool developed, unifying previously numerically integrated analysis, with a more robust application in the GMAT software, exploiting both advantages. Of course, many differences are present with respect to the purely numerically integrated solution, mainly concerning perturbations, eclipses events and thrust legs maneuver. However some considerations can be made given the results presented.

For instance, the two propulsion systems worked accordingly to the expected behaviour, both in terms of transfer time required and fuel mass needed for the maneuver. For the given amount of time imposed to perform the maneuver, in fact, a good percentage of the total time is spent in the thrust phase for the propulsion system, as the low-thrust doesn't allow for "impulsive-like" maneuver as opposed to the chemical one. This, however does not represent a disadvantage, since, when maneuvering, the spacecraft is moving into orbits which allow at the same time a gainful RAAN drift change, allowing the spacecraft to spend a lower time frame in the drift orbit. Completely opposite behaviour is shown for the chemical propulsion, as we expected.

Fuel mass consumption proves also to be plenty in the considered budget for the two different subsystems, even for the higher amount of correction imposed to the orbit. This, mainly, will come into hand with the analysis of the whole spacecraft lifetime, including station keeping maneuver to keep the satellite in its operational orbit. As the overall mission duration is of about 5 years (for the baseline), station keeping maneuver will be certainly needed, and a fraction of the propellant will then be necessary to perform them. There are, however some things to be considered from the physical point of view: the maneuver implemented in the case of the electric propulsion, as you may recall, relies on the switch of the yaw angle at the antinodes, allowing the effective thruster direction to change dynamically every half orbit. The assumption is, mainly, that the steering switch can be performed from the satellite point of view, meaning that there are not any impediment coming from this maneuver. There is the possibility, however, that the payload may suffer from incorrect pointing, or worse, that the payload will be in a sun-pointing situation, which is not acceptable for technological point-of-view, therefore

accurate attitude determination has to provide informations on whether or not the switch can be allowed, and in such cases, the satellite will only have to exploit half of the burning time previously accounted for.
Furthermore, considerations about the duty cycle have to be analyzed: the duty cycle analysis, in this work, is mainly weighted on the eclipse events, meaning that numerically integrated solutions do not account for a thrust period in case of umbra or penumbra. The technological point of view is then discarded, considering that the propulsion system is capable of performing the maneuver required, obviously. Further implementation needs to consider more accurate hardware modeling, in terms of thrust duration capabilities, and power decay during the subsystem lifetime.
Summarizing, both propulsion system are able to perform the maneuver in the desired way, with a relatively small amount of propellant, in the time considered. The problem, however, looks quite sensitive to the initial condition, so a fine tuning of these parameter is required (e.g.:choice of the commissioning days).
Ultimately,tools update will be then necessary to comply with mission requirements and operational constraints, still ongoing, but the preliminary analysis carried out pointed out that both propulsion systems are perfectly capable of carrying out the maneuver requested.

Bibliography

[1] ESA Space Debris Office. Esa's annual space environment report. Technical report, European Space Agency, Robert-Bosch-Strasse 5, Darmstadt, Germany, 2022.

[2] Donald J. Kessler, Nicholas L Johnson, J. c. Liou, and Mark Matney. The kessler syndrome: Implications to future space operations. 2010.

[3] IADC Space Debris Mitigation Guidelines.

[4] ESA. About Space Debris. `https://www.esa.int/Space_Safety/Space_Debris/About_space_debris`. [Online].

[5] eoPortal. About Space Debris. `https://www.eoportal.org/other-space-activities/orbital-debris#our-past-is-explosive`. [Online].

[6] G. Levrini and Attema E. The commissioning phase and the calibration/validation activities. bulletin 106, 2001.

[7] Samuel Pines. Uniform representation of the gravitational potential and its derivatives. *AIAA Journal*, 11, November 1973.

[8] NASA Goddard Space Flight Center. *GMAT Mathematical Specification*. 2020a edition, 2020.

[9] David A. Vallado. *Fundamental of Astrodynamics and Applications*. McGraw-Hill, 1 edition, May 1997.

[10] Velez C.E. Cappellari, J.O. and A.J. Fuchs. *Mathematical Theory of the GODDARD Trajectory Determination System*. 1 edition, 1976.

[11] L. G. Jacchia. Revised Static Models of the Thermosphere and Exosphere with Empirical Temperature Profiles. *SAO Special Report*, 332, May 1971.

[12] John T. Betts. Optimal low-thrust orbit transfers with eclipsing. *Optimal Control Applications and Methods*, 36(2):218–240, March 2015.

[13] O. Montenbruck and E. Gill. *Satellite Orbits: Models, Methods, and Applications*. Physics and astronomy online library. Springer Berlin Heidelberg, 2000.

[14] Beny Neta and David Vallado. On Satellite Umbra/Penumbra Entry and Exit Positions. *The Journal of the Astronautical Sciences*, 46(1):91–103, March 1998.

[15] Jonathan Aziz, Daniel Scheeres, Jeffrey Parker, and Jacob Englander. A smoothed

eclipse model for solar electric propulsion trajectory optimization. *Transactions of the Japan Society for Aeronautical and Space Sciences*, 17(2):181–188, 2019.

[16] Rodolpho Vilhena de Moraes. Combined solar radiation pressure and drag effects on the orbits of artificial satellites. *Celestial mechanics*, 25:281–292, 1981.

[17] D. Vokrouhlicky, P. Farinella, and F. Mignard. Solar radiation pressure perturbations for Earth satellites. 1: A complete theory including penumbra transitions. , 280(1):295–312, December 1993.

[18] V.A. Chobotov. *Orbital Mechanics*. AIAA education series. American Institute of Aeronautics and Astronautics, 1991.

[19] A. Ruggiero, Pierpaolo Pergola, Salvo Marcuccio, and Mariano Andrenucci. Low-thrust maneuvers for the efficient correction of orbital elements. *Proceedings of the 32nd International Electric Propulsion Conference, IEPC Paper*, pages 1–13, 01 2011.

[20] J. E. Pollard. Simplified Analysis of Low-Thrust Orbital Maneuvers:. Technical report, Defense Technical Information Center, Fort Belvoir, VA, August 2000.

[21] Theodore N. Edelbaum. Propulsion Requirements for Controllable Satellites. *ARS Journal*, 31(8):1079–1089, August 1961.

[22] Changxuan Wen, Chen Zhang, Yu Cheng, and Dong Qiao. Low-Thrust Transfer Between Circular Orbits Using Natural Precession and Yaw Switch Steering. *Journal of Guidance, Control, and Dynamics*, 44(7):1371–1378, July 2021.

[23] Lorenzo Casalino and Guido Colasurdo. Improved Edelbaum's Approach to Optimize Low Earth/Geostationary Orbits Low-Thrust Transfers. *Journal of Guidance, Control, and Dynamics*, 30(5):1504–1511, September 2007.

[24] Max Cerf. Low-Thrust Transfer Between Circular Orbits Using Natural Precession. *Journal of Guidance, Control, and Dynamics*, 39(10):2232–2239, October 2016.

[25] Jean Albert Kechichian. Reformulation of Edelbaum's Low-Thrust Transfer Problem Using Optimal Control Theory. *Journal of Guidance, Control, and Dynamics*, 20(5):988–994, September 1997.

[26] Mirko Leomanni, Gianni Bianchini, Andrea Garulli, and Renato Quartullo. Optimal Low-Thrust Orbit Transfers Made Easy: A Direct Approach. *Journal of Spacecraft and Rockets*, 58(6):1904–1914, November 2021. arXiv:2101.08160 [math].

[27] Jean A. Kéchichian. Analysis of optimal and near-optimal continuous-thrust transfer

problems in general circular orbit. *Acta Astronautica*, 65(5-6):879–891, September 2009.

[28] Jean A Kechichian. Optimal Low-Thrust Transfer in General Circular Orbit Using Analytic Averaging of the System Oynamics.

[29] Kathryn F. Graham and Anil V. Rao. Minimum-Time Trajectory Optimization of Low-Thrust Earth-Orbit Transfers with Eclipsing. *Journal of Spacecraft and Rockets*, 53(2):289–303, March 2016.

[30] Max Cerf. Fast solution of minimum-time low-thrust transfer with eclipses. *Proceedings of the Institution of Mechanical Engineers, Part G: Journal of Aerospace Engineering*, 233(7):2699–2714, June 2019.

[31] Vyacheslav Petukhov. Otimal MultiRevolutional Transfers Between Non-Coplanar Elliptical Orbits.

[32] Anil V Rao. A Survey of Numerical Methods for Optimal Control.

[33] John T. Betts. Survey of numerical methods for trajectory optimization. *Journal of Guidance Control and Dynamics*, 21:193–207, 1998.

[34] Haider Ali Biswas, Azmol Huda, Munnujahan Ara, and Ashikur Rahman. Optimal Control Theory and its Applications in Aerospace Engineering. *International Journal of Academic Research*, 3(2), 2011.

[35] John T. Betts. *Practical Methods for Optimal Control and Estimation Using Nonlinear Programming*. Society for Industrial and Applied Mathematics, second edition, January 2010.

[36] Md. Haider Ali Biswas, M. Huda, Munnujahan Ara, and Motahera Rahman. Optimal control theory and it's applications in aerospace engineering. *International Journal of Academic Research, Vol. 3, No. 2, Part II, pp. 349-357, 2011.*, 01 2011.

[37] Guzmán J.J. Longuski J.M. and Prussing J.E. *Optimal Control with Aerospace Applications*. Space Technology Library. Springer New York, 2013.

[38] Arthur E. Bryson and Walter F. Denham. Optimal programming problems with inequality constraints. ii - solution by steepest-ascent. *AIAA Journal*, 2:25–34, 1964.

[39] Tarunraj Singh. Fuel/time optimal control of the benchmark problem. *Journal of Guidance, Control, and Dynamics*, 18(6):1225–1231, November 1995.

[40] Michael P. Friedlander and Paul Tseng. Exact Regularization of Convex Programs. *SIAM Journal on Optimization*, 18(4):1326–1350, January 2008.

[41] Henri P. Gavin and Jeffrey T. Scruggs. Constrained optimization using lagrange multipliers. *CEE 201L, Uncertainty, Design and Optimization*, 2020.

[42] D. Bertsekas. *Constrained Optimization and Lagrange Multiplier Methods (Optimization and Neural Computation Series)*. Athena Scientific, 1996.

[43] CORNELIUS LANCZOS. *The Variational Principles of Mechanics*. University of Toronto Press, 1962.

[44] R. Tyrrell Rockafellar. Lagrange multipliers and optimality. *SIAM Review*, 35(2):183–238, 1993.

[45] L.S. Pontryagin. *Mathematical Theory of Optimal Processes*. Routledge, 1 edition, May 2018.

[46] C. Hargraves and Stephen Paris. Direct trajectory optimization using nonlinear programming and collocation. *AIAA J. Guidance*, 10:338–342, 07 1987.

[47] Alice E. Smith and David W. Coit. Penalty Functions. 1996.

[48] Thomas Bäck, D.B. Fogel, and Z. Michalewicz. *Handbook of Evolutionary Computation*. Number v. 1 in Computational intelligence library. Institute of Physics Pub., 1997.

[49] Robert M Freund. Penalty and Barrier Methods for Constrained Optimization.

[50] Edwin K P Chong. An Introduction to Optimization.

[51] NASA. In-Space Propulsion. https://www.nasa.gov/smallsat-institute/sst-soa/in-space-propulsion. [Online].

[52] Saccoccia G. Sabbadini M. and Buoso M. Electric propulsion technology programmes. *ESA Publications Division*, 2002.

[53] Sashikanth Rapeti. In-Space Electric Propulsion Systems - The Future of Spacecraft Propulsion Technologies. working paper or preprint, August 2021.

[54] Minduli C. Wijayatunga, Roberto Armellin, Harry Holt, Laura Pirovano, and Aleksander A. Lidtke. Design and guidance of a multi-active debris removal mission. *Astrodynamics*, February 2023.

A | Appendix A

Graphs report here are the one extracted from ESA's annual space environment report, carrying out an analysis of the current state of objects present in orbit classified in terms of object, mass and area.

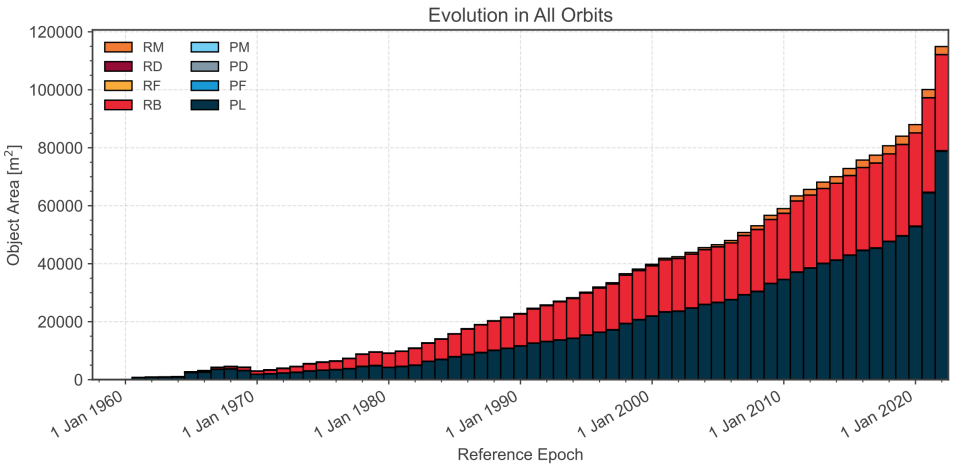

(a) Total number of object by class

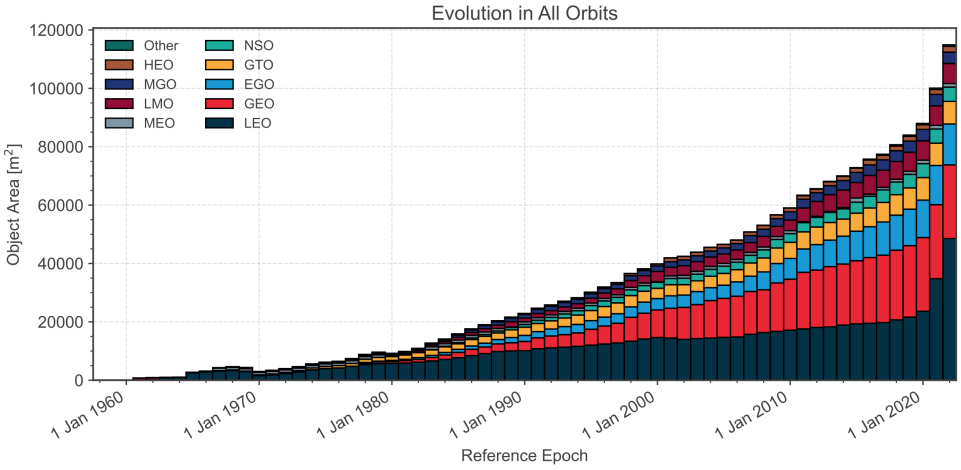

(b) Total number of object by orbit

Figure A.1: Evolution of the total Area of objects divided by class and by orbit

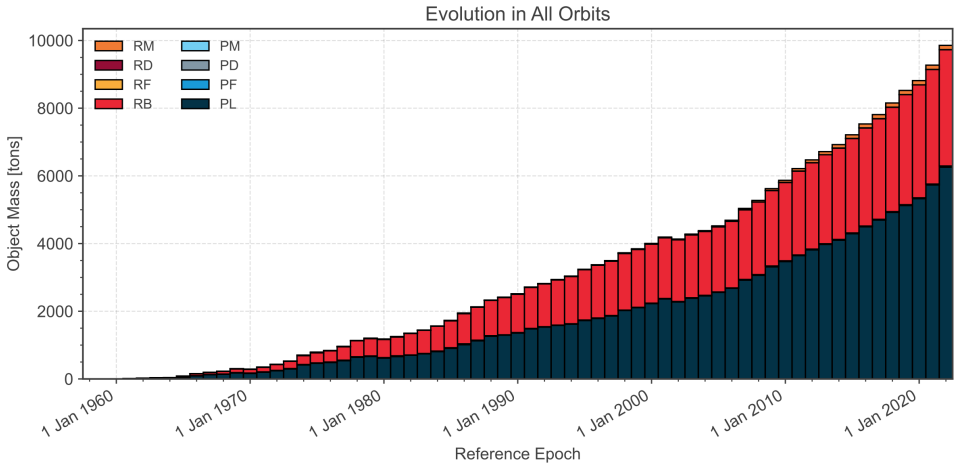

(a) Total number of object by class

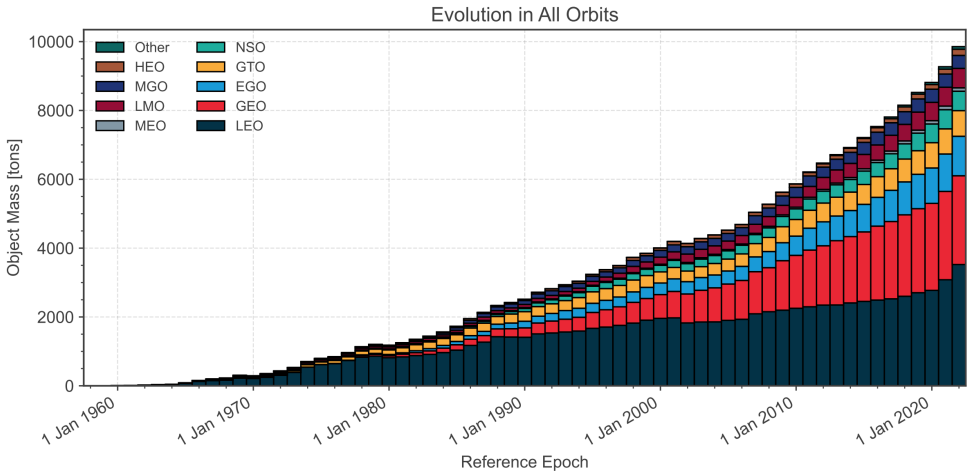

(b) Total number of object by orbit

Figure A.2: Evolution of the total Mass of objects divided by class and by orbit

B | Appendix B

Embedded Jacchia model for the computation of the atmospheric density. The model is used by default in the GMAT software.

Table 3. Tables for the computation of the semiannual density variation $\Delta \log_{10} \rho = f(z)\, g(t)$.

a) Table of f(z)

z (km)	f(z)	z (km)	f(z)	z (km)	f(z)
100	0.068	500	0.289	900	0.347
150	0.086	550	0.309	950	0.341
200	0.112	600	0.326	1000	0.332
250	0.142	650	0.338	1050	0.322
300	0.174	700	0.347	1100	0.311
350	0.207	750	0.351	1150	0.298
400	0.237	800	0.353	1200	0.285
450	0.265	850	0.351		

Figure B.1: Jacchia Roberts Atmoshpere model (1)

Table 4. Tables for the seasonal-latitudinal density variation $\Delta \log_{10} \rho = S P \sin^2 \phi$.

a) Table of the maximum half-range $S = 0.014(z - 90) \exp [-0.0013(z - 90)^2]$

z (km)	S	z (km)	S	z (km)	S
90	0.000	120	0.130	150	0.008
95	0.068	125	0.100	155	0.004
100	0.123	130	0.070	160	0.002
105	0.157	135	0.045	165	0.001
110	0.166	140	0.027	170	0.000
115	0.155	145	0.015		

b) Table of the phase $P = \sin (2\pi\Phi + 1.72)^*$

Day	P	Day	P	Day	P	Day	P
Jan. 1	±0.989	Apr. 1	∓0.129	June 30	∓0.994	Sept. 28	±0.086
11	±0.948	11	∓0.297	July 10	∓0.961	Oct. 8	±0.255
21	±0.880	21	∓0.456	20	∓0.900	18	±0.417
31	±0.786	May 1	∓0.602	30	∓0.812	20	±0.567
Feb. 10	±0.668	11	∓0.730	Aug. 9	∓0.699	Nov. 7	±0.699
20	±0.531	21	∓0.836	19	∓0.567	17	±0.812
Mar. 2	±0.378	31	∓0.918	29	∓0.417	27	±0.900
12	±0.214	June 10	∓0.972	Sept. 8	∓0.255	Dec. 7	±0.961
22	±0.043	20	∓0.998	18	∓0.086	17	±0.994
						27	±0.998

*Take the upper sign for the Northern Hemisphere, the lower for the Southern Hemisphere.

c) Table of $\sin^2 \phi$

ϕ	$\sin^2 \phi$	ϕ	$\sin^2 \phi$	ϕ	$\sin^2 \phi$
0°	0.000	30°	0.250	60°	0.750
5	0.008	35	0.329	65	0.821
10	0.030	40	0.413	70	0.883
15	0.067	45	0.500	75	0.933
20	0.117	50	0.587	80	0.970
25	0.179	55	0.671	85	0.992
				90	1.000

Figure B.2: Jacchia Roberts Atmoshpere model (2)

C | Appendix C

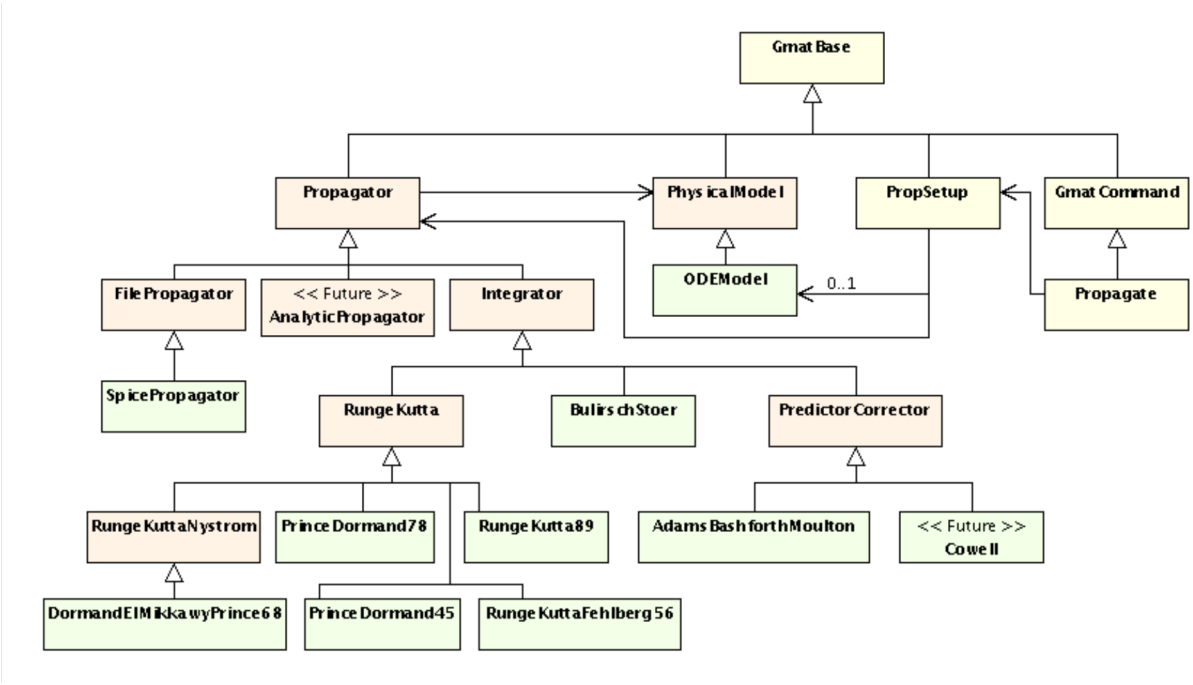

Figure C.1: GMAT Integrators